Validation of aeroelastic dynamic model of ~~Active Trailing Edge Flap~~ active trailing edge flap system tested on a 4.3 MW wind turbine

Andrea Gamberini[1,2], Thanasis Barlas[2], Alejandro Gomez Gonzalez[1], and Helge Aagaard Madsen[2]

[1]Siemens Gamesa Renewable Energy A/S, Brande, Denmark
[2]DTU, Dept. of Wind and Energy Systems, Roskilde, Denmark

Correspondence: Andrea Gamberini (andgam@dtu.dk)

Abstract. Active Trailing Edge Flap (ATEF) is a promising technology for ~~Wind Turbine load reduction and AEP improvement. However, this technology still needs extensive field validations to prove the reliability of the ATEF aeroelastic modeling codes .~~ controlling wind turbine loads and enhancing energy production. The integration of this technology in the design of commercial wind turbines requires dedicated flap aeroelastic models, as aeroelastic simulations have an essential role in the wind turbine design process. Several aeroelastic codes developed specific flap modules. However, these models were only partially validated, with the risk of incorrect performance prediction that could jeopardize the development of commercial wind turbines equipped with ATEF. This article describes the validation of the ~~dynamic response of the ATEF~~ flap aeroelastic models developed ~~for the BEM-based solvers~~ by two aeroelastic codes, HAWC2 and BHawC, aiming to reduce the uncertainty of the dynamic response of the two flap aeroelastic models. The validation ~~relied~~ relies on field data from a 4.3 MW ~~Wind Turbine (WT)~~ wind turbine equipped with an ~~ATEFS~~ ATEF on one blade and operating in normal power production. The validation ~~consisted of three phases~~consists of three steps. At first, ~~video recording of the ATEF deflection during WT operation allowed the tuning~~ the actuator models of the flap are tuned based on the video recording of the flap ~~actuator model. In the second phase, the aerodynamic flap model was~~ deflections. The aerodynamic flap models are tuned and validated ~~through the lift coefficient (Cl) transients measured~~ in the second step through the mean lift coefficient transient response. The lift coefficient is obtained with an innovative autonomous add-on measurement system placed on the blade in the middle of the spanwise extension of the ~~ATEF~~flap. Finally, the ~~aeroelastic ATEF model was~~ whole aeroelastic ATEF models are validated based on the ~~blade root moment (BMrM) transients over three months , from October to December 2020,~~ mean blade-to-blade moment transient response obtained from three months of field data with varying weather conditions. The validations ~~showed that the simulations transient of Cl and MBrM are in good agreement with the corresponding measured transients, with a maximum difference for the blade-to-blade MBrM transients below 1% of the mean blade load during flap activation and below 1.7% during flap deactivation. An analysis of the possible root causes of these differences suggested additional measurements~~ show a good agreement between the simulated and measured mean transient responses. Furthermore, additional measurements are suggested to improve the ~~ATEF~~ flap model tuning. The validation ~~confirmed that the aeroelastic ATEF~~ confirms that the studied aeroelastic models provide a reliable and precise estimation of the dynamic impact of the flap actuation on the wind turbine

during flap actionaerodynamics and loading, a fundamental step in the safe implementation of the active flap in the design of commercial wind turbines.

1 Introduction

In recent years, the steady growth in the size of utility-scale Wind Turbines (WT) wind turbines led by the pursuit of lower levelized cost of energy resulted in a significant increase in the load carried by the WT wind turbine components. One of the most promising technologies to mitigate the load increase consists of actively controlled flaps located at the blade trailing edge, the so-called Active Trailing Edge Flap (ATEF). From the pioneering works of Van Wingerden et al. (2008), Andersen (2010), Lackner and Van Kuik (2010),Aagaard Madsen et al. (2010) and Castaignet et al. (2011), to some of the more recent research by Bergami and Poulsen (2015), Barlas et al. (2016), Fischer and Aagaard Madsen (2016) and Bernhammer et al. (2016), several studies support that the integration of the ATEF in the WT design has the potential trailing edge flaps can be actively controlled to reduce extreme and fatigue loads . in several wind turbine components. For example, Ungurán and Kühn (2016) estimates a 10% reduction in the flapwise blade root bending moment and a 6% reduction in the tower side-side bending moment with an individual flap control strategy. These load reductions can be exploited to lower the components' cost or to increase the AEPincrease the energy production, as shown by Pettas et al. (2016) and Abbas et al. (2023), which estimated a potential reduction of the levelized cost of energy of 1.3%.

Despite the consensus on Currently, the design of commercial wind turbines heavily relies on low-fidelity aeroelastic models thoroughly validated with field measurements. Therefore, the field validation of the flap aeroelastic models is paramount for integrating the active flap into the wind turbine design. An extensive validation ensures the soundness of the simulation results, reducing the uncertainty and associated risks (and costs) that could jeopardize the introduction of active flaps in the potential benefits of active flaps in load reduction, the full-scale validation of ATEF aeroelastic engineering models and their potential load reduction is limited. Validating these models is challenging. An wind turbine design.

Flap models have been developed in most of the aeroelastic codes, like HAWC2 Larsen and Hansen (2023), FAST Jonkman et al. (2005) or Bladed Bossanyi (2013). However, their field validation is limited, particularly at commercial scale. This limitation arises mainly from the substantial financial investment needed for experimental testing activities, particularly in publicly funded research, and the absence of an existing reliable design of the active flap system that limits the interest from the private sector. When measurement data is missing, the aeroelastic codes are usually validated by comparison against higher fidelity models, which are better trusted. Prospathopoulos et al. (2021) performed an extensive code-to-code comparison of various existing models for simulating active flaps on rotating bladeswas performed in Prospathopoulos et al. (2021), where state-of-the-art Blade Element Momentum (BEM) models (hGAST, HAWC2, and FAST) were compared with higher fidelity models, including free-wake lifting line (GENUVP) and fully resolved Computational Fluid Dynamics (CFD) models (MaPFlow and FLOWer). The comparison concluded that the BEM models cannot reproduce the correct distribution of the local thrust forces in the proximity of the flap edges because they neglect the 3D effects originated by the vorticity trailed from the edges and along the span of the flap section. However, these BEM models reasonably estimate the impact of an oscillating flap on the in-

tegrated overall thrust when the oscillating frequency is 1P. This result is explained by the over-prediction of the flap impact in the flap region being overall compensated by the flap impact under-prediction in the blade regions near the flap edges. With the increase of the flap ~~activation~~ actuation frequency, BEM model accuracy decreases. Finally, the study showed that modifying the BEM models to account for 3D effects due to the vorticity trailed from the flap edges (HAWC2 with Near Wake model and modified FAST) improved their prediction of both the local and the global impact of the flap on the thrust force.

~~ATEF subsystem validations have also been conducted through~~ The code-to-code validation is a powerful tool. However, experimental measurements are still necessary to verify that the calculated behavior of the aerodynamic forces reflects reality as the CFD calculations still present limitations Ferreira et al. (2016). Therefore, ATEF subsystem validation was carried out through a variety of experimental methods, including wind tunnel tests ~~(e.g. Barlas et al. (2013))~~ Barlas et al. (2013) and outdoor rotating rig experiments Gonzalez et al. (2020) Barlas et al. (2018). Recently, 3-dimensional lab-scale tests were performed within the large wind tunnel of the TU Berlin on BeRT, a 3 m diameter research turbine equipped with ATEF on each blade. The ability of different controllers employing trailing edge flaps to reduce fatigue (Bartholomay et al. (2022)) and extreme (Bartholomay et al. (2023)) flapwise blade root bending moments were assessed meanwhile providing datasets for future validation of numerical models. Regarding full-scale validation, only three field tests have been reported so far. These tests include the Sandia field test on a Micon 65/13 turbine (115 kW) Berg et al. (2013), the DTU and Vestas test on a V27 (225 kW) turbine Castaignet et al. (2014), and the Siemens Gamesa Renewable Energy (SGRE) and DTU tests on an SWT-4.0-130 (4.0 MW) turbine as part of the INDUFLAP2 project Gonzalez et al. (2020). Although these field tests confirmed the potential of active flaps in controlling aerodynamic loads, they also highlighted the need for further development and validation of numerical models for ATEF.

To address this gap, between 2019 and 2022, SGRE and DTU carried out the Validation of Industrial Aerodynamic Active Add-ons (VIAs) project ~~was carried out between 2019 and 2022 by SGRE and DTU~~to further develop, demonstrate, and validate active flow technologies for rotor blades at full scale, as described in Gomez Gonzalez et al. (2022). As part of this project, a prototype wind turbine (named as Prototype in this paper) with a rated power of 4.3 MW and a diameter of 120m ~~(PT)~~ was equipped with ~~an pneumatically activated~~ a pneumatically actuated ATEF on a single blade. From May 2020 to February 2021, extensive testing of the active flap was conducted with ~~different actuation strategies and flap deflection angles. The~~ both time-fixed on-off flap actuation (shifting between two different flap positions at fixed time intervals) and 1P cyclic on-off flap actuation (cyclic activation of the flap both in-phase and counter phase with the blade azimuthal position). In time-fixed on-off actuation, the flap impacted the mean blade root flapwise bending moment between 3% and 20%, depending on the flap actuation level and wind speed. In 1P cyclic actuation, the flap showed a potential reduction of 13% on the fatigue blade root flapwise bending moment. Furthermore, the data collected in VIAs field tests allowed Gamberini et al. (2022) to validate for flap stationary ~~activation~~ activated state the ATEF model of the aeroelastic engineering tools BHawC (Fisker Skjoldan (2011)) and HAWC2 (Larsen and Hansen (2023) and Aagaard Madsen et al. (2020)). The study relied on the measurements of the ~~10 minutes~~ 10-minute mean and maximum blade bending moments at the root of the three blades of the ~~PT~~ Prototype collected with the flap locked in a fully activated or deactivated position. A one-to-one validation approach was followed, where the aeroelastic simulations were performed under the wind conditions measured during the test campaign. The validation showed

that the BHawC and HAWC2 tools equipped with ATEF agree with each other (difference within 2% for ~~max~~ maximum and mean blade loads) and can estimate the blade loads with accuracy within ±5% for ATEF stationary ~~activation~~ activated state.

~~The subsequent step in the ATEF model validation is the comparison of the aeroelastic response to the step actuation of the flap~~After the validation of the ATEF aeroelastic model under a stationary flap state, the subsequent step is validating the model's dynamic response to flap actuation. In this article, the transient response of the BHawC and HAWC2 ATEF models ~~during flap~~ to flap actuation (activation and deactivation) is investigated and compared to the field data ~~gathered in~~ obtained from the VIAs project. ~~The purpose of this validation is~~ BHawC and HAWC2 ATEF have similar but different aerodynamic flap models, with the latter not only computing the 2D steady aerodynamic properties of a flap section but also directly computing the unsteady aerodynamic forces and pitching moments due to arbitrary deflection and motion of the flap. The validation is focused only on the step flap actuation because the simple flap actuation system of the Prototype did not allow more complex controller strategies, like a sinusoidal flap actuation. The validation aims to enable reliable aeroelastic modeling of the load reduction strategies based on the actuation of trailing edge flaps, a fundamental milestone in the design of future ~~WT~~ wind turbines equipped with ATEF.

In this article, section 2 resumes the active flap system installed on the ~~PT~~Prototype, and section 3 describes the ~~PT~~ Prototype aeroelastic model developed in BHawC and HAWC2 together with the structure of the ATEF model. The validation of the aeroelastic model is conducted in ~~steps. The first step is tuning the actuator model~~ three steps, schematically depicted in Figure 3. Step 1: flap actuator model tuning, described in section 4. This step covers both the pneumatic system and flap sub-system response. ~~Then the aerodynamic model is initially validated with a 3 hours~~ Step 2: aerodynamic model initial validation, described in section 5. It is based on a three-hour field campaign where the lift coefficient (Cl) was measured on a specific blade section of the ~~PT~~Prototype. Step 3: extended model validation, described in section ~~5. Finally, section 6describes how the model~~ 6. The flap aeroelastic model built and tuned in the previous steps is validated with a ~~three months~~ three-month field campaign, covering a broad range of wind conditions but relying only on blade root loads. ~~The~~ Section 7 briefly explores the impact of accounting for 3D effects due to the vorticity trailed from the flap edges by activating the Near Wake model in HAWC2. Finally, the overall results are ~~then~~ discussed in section 8.

2 Flap system and measurement setup

The VIAs project implemented an ATEF system on a single blade of the SGRE ~~PT~~ Prototype located at the Høvsøre test site ~~in the northwest of Denmark~~(DK). Gomez Gonzalez et al. (2022) provides a detailed description of the active flap system, which consisted of a pneumatic supply system located in the hub and connected with a hose to the active flap. The flap, shown on the left of Figure 1, was placed on the trailing edge of the outer 20 meters of the blade, between 64% and 98% of the blade radius. The pneumatic supply system ~~had a~~ consisted of an accumulator tank, a pump system, and a pressure valve. A remotely programmable control ~~that regulated the~~ system regulated the target air pressure value and the pressure ~~in the hose via a pressure valve . The air pressure~~ valve activation state (open or "to atmosphere"). The flap system allowed two actuation phases: in the activation phase, the pressure valve is open, the pressure in the hose ~~controlled the flap movement; the~~ rises to the target value,

and the flap deflects to increase the local lift; in the deactivation phase, the pressure valve opens to the atmosphere, the pressure in the hose and the flap drops to zero, and the flap returns to a load neutral position. Therefore, the controller signal of the pressure valve state, named the flap control state signal in this paper, controlled the flap actuation state. Meanwhile, the target air pressure value defined the maximum flap deflection: the higher the pressure, the higher the flap deflection ~~amplitude.~~ and the consequent local lift increase. The VIAs field campaign tested three target air pressures: low, middle, and high. The difference in angular flap deflection between the low and high actuation pressure state corresponded with approximately $10\,\mathrm{deg}$. However, sufficient data for the flap model validation was collected only with middle pressure. Throughout the field campaign, the ~~PT~~ Prototype was equipped with a ~~Data Acquisition System (DAS)~~ data acquisition system that continuously logged operational parameters, such as power, pitch, and rotor speed, with a 25 Hz sampling rate. The same sampling rate was used to measure the flapwise and edgewise bending moments of all three blades by strain gauges located in the blades at $3\,\mathrm{m}$ from the root. Also, the pressure at the pressure valve in the hub was recorded and integrated into the ~~DAS~~data acquisition system. Furthermore, a met mast located approximately 2.5 D ($300\,\mathrm{m}$) in front of the ~~WT~~ wind turbine provided the wind speed and direction at three different heights, the atmospheric pressure, the temperature, and the humidity.

In June 2020, an inflow and pressure measurement system was temporarily added to the ~~PT~~ Prototype to measure the aerodynamic properties at a specific ATEF section, as described in Madsen et al. (2022) and showed in the central photo of Figure 1. The system, developed by DTU, consisted of an inflow 5-hole Pitot tube sensor, a belt with 15 pressure taps, and an autonomous data acquisition and transmission system (flyboard). Both Pitot tube and flyboard were installed on the blade leading edge at $50\,\mathrm{m}$ from the hub flange, in the middle of the spanwise extension of the ~~ATEF~~flap. The pressure belt was wrapped around the blade at a spanwise position of $49\,\mathrm{m}$. The inflow and pressure measurement system provided data with a 100 Hz sampling rate that was synchronized with the ~~PT~~ Prototype measurement data by the recorded GPS time. A close view of the pressure belt and flyboard is shown in the bottom right photo of Figure 1.

Additionally, two couples of small plastic fins were installed near the pressure belt location to analyze the ATEF deflection visually. The fins of each couple lay aligned on the same blade section, with the two couples spaced around $0.5\,\mathrm{m}$ apart spanwise. For each couple, one fin was attached to the moving ATEF and the other to the blade structure. A GoPro camera was installed closely to record the flap deflection using the fins as reference points, as shown in the top right picture of Figure 1.

3 Aeroelastic setup

3.1 BHawC model

SGRE has internally developed and validated the aeroelastic engineering tool BHawC, based on the Blade Element Momentum (BEM). ~~SGRE has furthermore developed a ATEF Module~~ Furthermore, SGRE has developed an ATEF module to model the flap aerodynamic and actuator system. The model uses the instantaneous value of the flap angle (or flap state) to interpolate the instantaneous steady two-dimensional (2D) aerodynamic characteristics of the flap sections from a pre-generated set of 2D steady aerodynamic properties provided for a range of flap angles (or flap states). These properties are then provided to the global wind turbine model to replace the 2D aerodynamic blade characteristics in the blade sections equipped with flaps.

Figure 1. Left photo: Active flap placed on the trailing edge of the blade of the ~~SWT-DD-120 turbine~~ Prototype at the Høvsøre test field. Central photo: Installation of the flyboard and pressure belt in June 2020. Bottom right photo: Close look at the flyboard and the pressure belt. Top right photo: Camera and fins installed to measure the flap deflection. Photos courtesy of SGRE and DTU.

The BHawC model adopted in this paper was provided by SGRE and fine-tuned by the authors in Gamberini et al. (2022) where ~~they showed the aeroelastic simulations were~~ the aeroelastic model was able to estimate the ~~PT~~ Prototype operational parameters with ~~an accuracy of~~ a maximum error lower than $\pm 3\%$ and blade loads within $\pm 2\%$ for the ~~condition of stationary flap~~ flap in stationary state. The current paper covers the tuning and validation of the ATEF ~~Module actuator and the part of the aerodynamic model responsible for the aeroelastic response to the flapactuation~~actuator and aerodynamic model during the dynamic actuation of the flap.

3.2 HAWC2 model

HAWC2 is the BEM aeroelastic engineering tool developed by DTU Wind. It ~~is based on BEM and models the unsteady aerodynamics associated with the active flaps with~~ models the ~~Beddoes-Leishman type ATEFlap dynamic stall model Bergami and Gaunaa (~~ active flap with ATEFlap, an advanced "engineering" model that not only computes the 2D steady aerodynamic properties of a flap section but also directly computes the unsteady aerodynamic forces and pitching moments due to arbitrary deflection and motion of the flap. Under the assumption of plane wake separation, trailing edge stall separation, and uniform upwash velocity along the chord, ATEFlap can describe the dynamic of the forces related to the flow separation and the effects of the vorticity shed into the wake (Bergami and Gaunaa (2012)).

The authors tuned the HAWC2 model of the SGRE ~~WT prototype~~ Prototype in Gamberini et al. (2022), based on the BHawC model, obtaining negligible code-to-code differences (~~max~~ maximum difference below 1%) for mass properties and ~~WT~~ wind turbine operational parameters and a ~~max~~ maximum difference within 4% for the blade loads. For the ATEFlap model, the suggested values of the coefficients for the indicial response exponential function and the exponential potential flow step response

were used. These parameters were tuned to describe the step response of the NACA 64-418 ~~profile~~ airfoil (18% thickness) that can be considered an acceptable approximation for the modeled ~~ATEF~~flap.

3.3 Modeling of the Flap system

The ATEF system installed on the ~~PT was~~ Prototype is simplified as a controlled pneumatic system ~~that regulated~~ regulating the pressure inside ~~a~~ the hose connected to the ~~flap located on the trailing edge of one blade~~active flap. Increasing the air pressure ~~inflated~~ inflates the hose that ~~deflected~~ deflects the flap. The flap deflection ~~changed the blade profile~~ changes the blade section shape, consequently modifying the local aerodynamic forces and affecting the loading of the whole ~~PT.~~Prototype

In the ATEF aeroelastic model, depicted in Figure 3, the pneumatic system and the flap structure ~~were~~ are merged in the actuator model. This model ~~linked~~ directly links the controller signal ~~directly~~ of the flap state to the flap deflection, disregarding the air pressure signal. This simplification ~~was~~ is possible because the ~~pneumatic system did control~~ controller system controlled only the final pressure value ~~but did not control the pressure transient. This transient~~ and the pressure valve actuation time. The variation of the air pressure inside the hose after the valve actuation depended only on the ~~pneumatic system layout . Therefore~~ layout of the pneumatic and flap systems after the valve (for example, the length, diameter, and material of the hose and the stiffness of the flap). Therefore, the air pressure and the ~~consequent~~ corresponding flap deflection were expected to have a ~~constant transient for every defined activation pressure value~~similar transient response for each pressure valve actuation.

The actuator model ~~provided~~ provides the flap deflection to the aerodynamic model that ~~computed~~ computes the dynamic aerodynamic properties of the flap section, which is needed by the aeroelastic code to ~~compute the PT~~ calculate the Prototype loads. In both codes, the ATEF aerodynamic model ~~relied on the~~ relies on the flap airfoils' stationary lift and drag coefficient (Cl and Cd) ~~curves of the flap profiles for both active and not active~~ data for active and deactivated flap states. The flap was installed over a longitudinal blade section with thickness ranging from 24% to 18% of the chord; therefore, the aerodynamic characteristics of the flap airfoils with thickness between 24% and 18% are needed. SGRE provided the aerodynamic characteristics of the 21% thickness ~~flap profile~~airfoil of the blade equipped with the flap. Similarly to the method described in Gomez Gonzalez et al. (2018), SGRE measured the aerodynamic characteristics in a wind tunnel campaign performed at the Low-Speed Low-Turbulence wind tunnel facilities of the faculty of aerospace of TU Delft. The measurements, most of them run at a Reynolds number of ~~mainly~~ 4 million, focused on the 21% thickness ~~profile~~ airfoil where three different shapes of the deflected flap were modeled with a corresponding fixed add-on. The measurements provided the aerodynamic characteristics for the flap that was not active ~~, which was activated with low pressure and activated with high pressure~~and active at low and high actuation pressures. The data for middle ~~activation pressure were instead~~ actuation pressure are obtained by interpolation, as previous tests in the VIAs project showed a linear relation between flap deflection and pressure for the studied ATEF system. ~~To fully simulate the flap on the PT, the~~ The aerodynamic characteristics of the 24% and 18% thickness ~~flap profiles were needed. They were~~ airfoils are computed assuming that the same flap deflection leads to the same lift and drag variation across the family of flap ~~profiles~~airfoils. Under this assumption, from the 21% thickness ~~profile~~airfoil, the lift and drag increases due to a specific flap deflection ~~were~~ are calculated as a function of the angle of attack. These ΔCl and ΔCd ~~were~~ are added to the 24% and 18% thickness ~~profile~~ airfoil properties after being linearly scaled to adjust to the actual chord

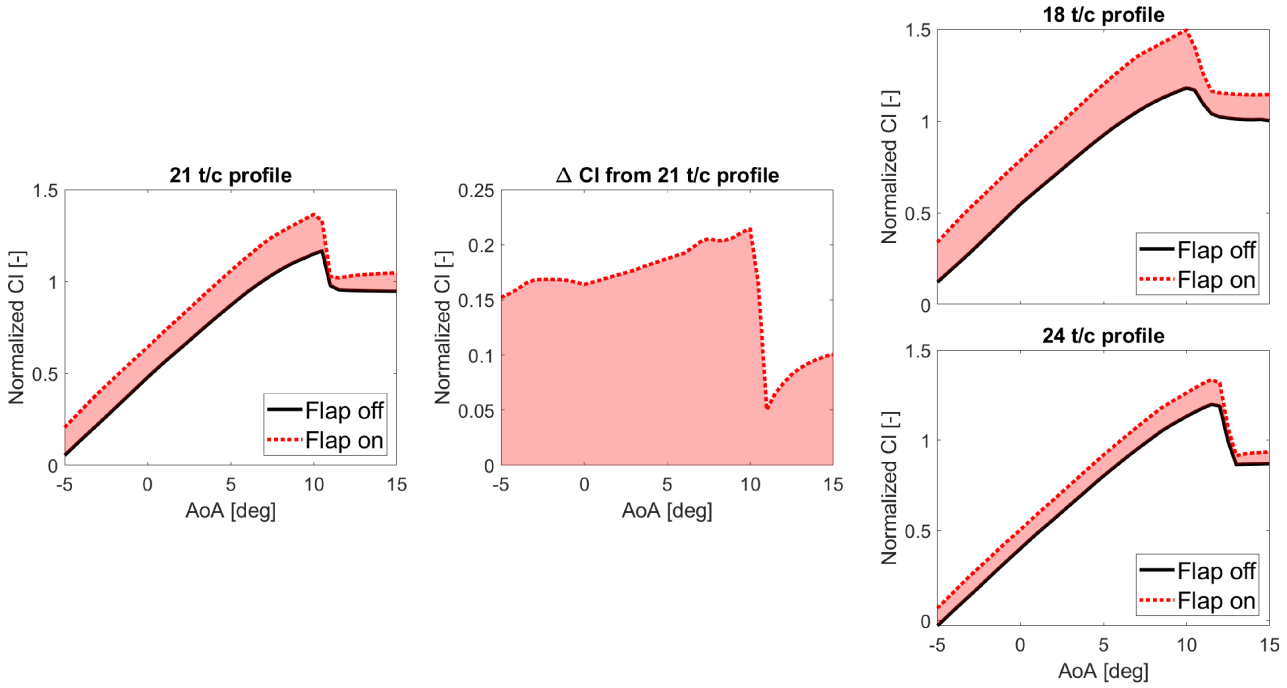

Figure 2. Left: Normalized Cl ~~curve~~ versus angle of attack of the 21% thickness ~~profile~~ airfoil with flap not active (black) and ~~flap~~ active at low pressure (red dotted line). Center: ΔCl from the 21% thickness ~~profile~~ airfoil due to flap activation. Right: Normalized Cl ~~curve~~ versus angle of attack of 18% (Top) and 24% (Bottom) thickness ~~profile~~ airfoils with flap active at low pressure (red dotted line) obtained by adding the scaled ΔCl from the 21% thickness airfoil to the curves with flap not active (black lines).

length of the new ~~profiles~~airfoils. Figure 2 shows an example of curves of the normalized Cl ~~curves~~ versus angle of attack for flap not active (black line) and ~~flap~~ active at low pressure (red line) of the 21% (left), 18% (top right), and 24% (bottom right) thickness ~~profiles~~airfoils. It also shows the ΔCl obtained from the 21% thickness ~~profile~~ airfoil (center). The ATEFlap model of HAWC2 ~~required~~ requires the aerodynamic properties to be in a specific format, where aerodynamic coefficients ~~were~~ are given as a function of the angle of attack and the angle of flap deflection. This format ~~was~~ is obtained utilizing the Preproc ATEFlap tool. ~~BHawC and~~ The BHawC flap model directly provides the instantaneous stationary 2D aerodynamic properties to the global wind turbine model. Instead, the HAWC2 ~~aerodynamic models assume a linear proportional relationship between the flap deflection and the variation of the static Cl and Cd. Both codes derive the dynamic properties with a partially different approach, mainly due to different dynamic stall models, properties that are then passed to the global WT aeroelastic model.~~ ATEFlap model computes already the unsteady effects due to flow separation and the vorticity shed into the wake, providing the instantaneous dynamic aerodynamic properties to the global wind turbine model.

~~The tuning and validation of the ATEF model was performed in three steps. At first, the actuator model was tuned to match the actual flap deflections obtained on the PT for the required activation flap pressure. The second step consisted of an initial validation based on the Cl measurements obtained from the flyboard installed at the PT flap location in a three hours long field~~

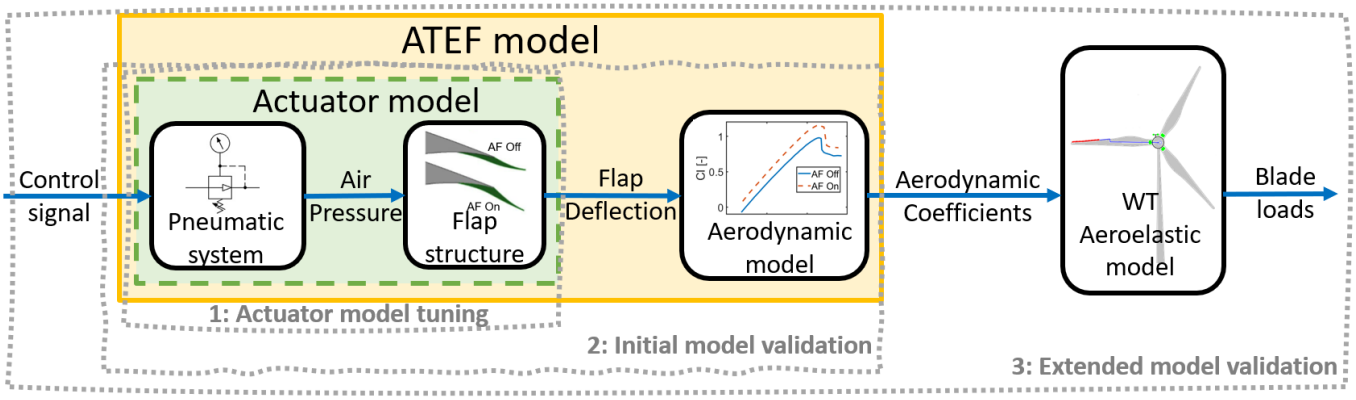

Figure 3. Structure of the ATEF aeroelastic model implemented in BHawC and HAWC2. Dotted-edged rectangles indicate the model elements involved in the three validation steps.

~~campaign. Finally, the ATEF aerodynamic model was validated based on blade root load transients measured in a three months long field test.~~

4 Actuator model tuning

To validate the aerodynamic model, a reliable flap actuator model ~~was~~ is needed to compute the ~~flap position and its transient~~position and motion of the flap. In this paper, the ~~development and~~ tuning of the flap actuator model ~~were~~ is obtained by the analyses of video recordings of the ~~PT~~ Prototype flap actuation.

In June 2020, a GoPro camera and two sets of plastic ~~fins~~ fin were temporarily installed on the ~~PT~~ Prototype blade. The camera captured the movements of the flap during its activation and deactivation under three distinct ~~activation~~ actuation pressure levels (low, middle, and high) and two operational states of the wind turbine: idling mode and normal operation at 6 rpm. Each combination was repeated four times to ensure data reliability. The video analysis and modeling tool Tracker (Brown et al. (2023)) ~~was~~ is utilized to extract the flap deflection in each video by tracking the relative position of the two fins during the flap activation and deactivation. For each combination, the four recorded cases consistently ~~yielded~~ yield a similar flap deflection ~~transient~~ response during flap activation; their binning and normalization ~~resulted~~ result in the characteristic flap activation deflection ~~transient~~ response (activation deflection curve) that ranged between 0 (flap not active) and 1 (flap fully deployed). The characteristic flap deflection ~~transient~~ response for deactivation (deactivation deflection curve) ~~was~~ is obtained with a similar process.

The comparison of the flap deflection ~~transients showed~~ responses shows a substantial overlap of the curves obtained for middle and high ~~activation~~ actuation pressure, with the low-pressure case being slightly faster. Although increasing the ~~activation pressure resulted~~ actuation pressure results in higher flap deflection, the normalized flap deflection ~~transient remained independent of pressure from middle activation pressure and above~~curve is independent of the activation pressure for middle and above

pressure values. Furthermore, the flap ~~displayed~~ displays a slower activation and a faster deactivation when the ~~WT was~~ wind turbine is in normal operation compared to the idling state. The latter behavior can be attributed to the effect of the aerodynamic pressure distribution on the blade section, which generates an aerodynamic force ~~that opposes~~ opposing the flap deflection during activation and ~~supports~~ supporting it during deactivation. The magnitude of this aerodynamic force, higher in the normal operation state compared to the idling state, directly affects the time required for full activation and deactivation, with higher forces resulting in slower activation and quicker deactivation.

In modeling the flap actuator, ~~we assumed~~ it is assumed that the activation and deactivation curves ~~were~~ are independent of the ~~actual activation~~ target actuation pressure. This assumption ~~was~~ is valid for high and middle ~~activation pressure scenarios which are~~ actuation pressure scenarios covering most of the available ~~PT~~ Prototype field data. The actuator model should also include the impact of the aerodynamic loads on the flap dynamic, which varies in function of the wind speed and ~~WT~~ wind turbine operational state. Therefore, ~~we selected~~ the middle and high-pressure deflection ~~transients~~ curves for normal production were selected, assuming a negligible change in the impact of the aerodynamic load ~~change~~ around the measured operative condition. The neglection of the impact of the aerodynamic loads on the total flap deflection ~~was also neglected~~ is also based on the results from Gamberini et al. (2022), where the stationary flap properties were validated for a wide range of wind speeds.

On the ~~PT~~ Prototype pneumatic system, the signal of the flap state controller was not recorded. Therefore, the pressure channel ~~was used to initially identify the~~ is initially used to identify the flap controller activation time, assuming no delay between the controller activation and the opening of the pressure valve. The flap actuator ~~was~~ is finally modeled as a simple second-order transfer function without poles. A fourth-order polynomial function was added to improve the similarity with the deflection curve data. In Figure 4a, the activation deflection curve for middle and high actuation pressure (black line) with the error band of ~~1~~ one standard deviation (std) is compared with the modeled second-order transfer function (blue dotted line), and the improved model with the fourth-order polynomial function (red dashed line with circles). Similarly, Figure 4b compares the experimental and modeled flap deactivation ~~transients~~curves.

5 Initial ATEF ~~Aerodynamic~~ aerodynamic model validation~~on a WT blade section~~

The aerodynamic model of the ATEF aeroelastic module ~~was~~ is initially validated for a single ~~PT~~ Prototype blade section equipped with the active flap. This validation ~~relied on a three hours~~ relies on a three-hour measurement data set ~~focused on one~~ with an almost constant wind speed. It ~~compared the transient~~ compares the transient response of the lift coefficient measured on the ~~PT blade~~ Prototype blade section with the Cl transient response curve calculated via aeroelastic simulations during the flap activation and deactivation. ~~The validation furthermore included the comparison of the~~ In addition, the validation includes comparing the measured and simulated transient responses of the blade-to-blade flapwise bending moment at the root of the blades.

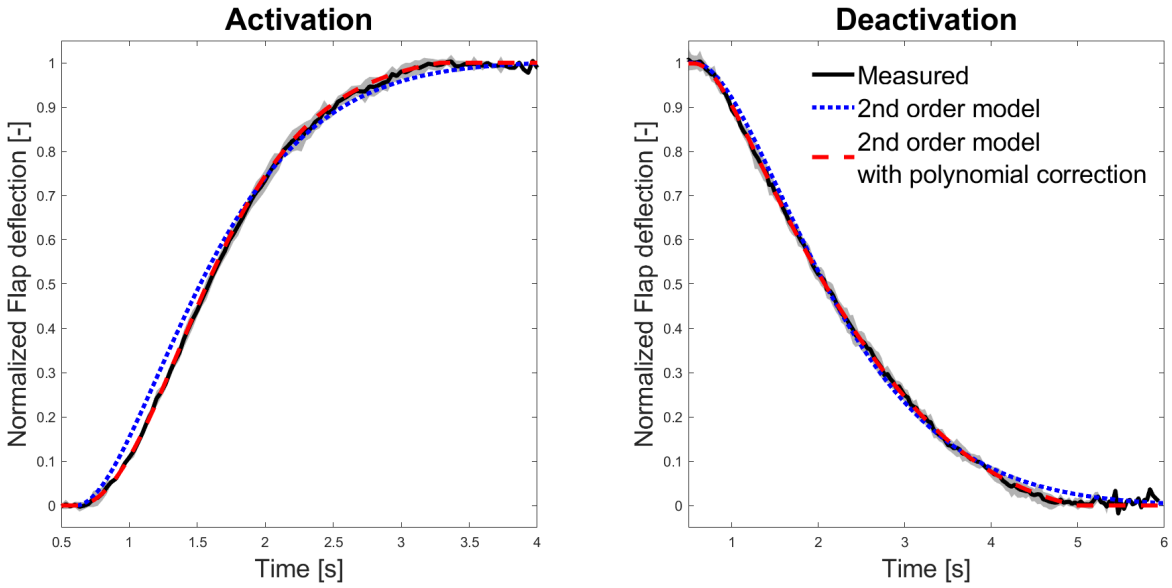

Figure 4. Normalized flap deflection ~~transients~~ curves measured with the video tracking (black line), obtained from the second-order transfer function model (blue dotted line) ~~,~~ and from the second-order transfer function model fine-tuned with a fourth-order polynomial function (red dashed line with circles) for flap activation (figure a) and deactivation (figure b). The measured lines are shown with the mean value line enveloped by the grey ~~1~~ one std error band

5.1 Measurements

In June 2020, an inflow and pressure measurement system was temporarily mounted on the ~~PT~~ Prototype in the middle of the blade span equipped with the active flap for around one day (Madsen et al. (2022)). The measurement system comprised a pressure belt with 15 taps, a 'flyboard' with the data acquisition system, and a five-hole Pitot tube measuring the local inflow to the blade section. The data acquisition system in the flyboard sampled the data from the pressure scanners and the five-hole Pitot tube with a sampling rate of 100 Hz. The captured raw data from the flyboard and pressure belt were processed and converted into quantities of interest. This process ~~includes the calibration of the~~ included calibrating the Pitot tube pressure data and conversion into two flow angles (inflow ~~angle and sideslip angle~~and sideslip angles) and a velocity. The inflow measurement quantities were further corrected to transform the Pitot tube inflow angle into the airfoil angle of attack ~~AoA~~ and relative velocity. This transformation was based on 2D CFD simulations performed by SGRE on the airfoil section for zero and full flap states, where the flow velocity and angle at the point of measurement of the Pitot tube were extracted as a function of the geometric angle of attack~~(AoA)~~, see Madsen et al. (2022). The pressure belt data was integrated into 2D aerodynamic forces by chordwise trapezoidal integration of the pressures, where a trailing edge pressure was added as an average of the two nearest points. The local pressure and lift coefficients (Cl) were calculated using the corrected dynamic pressure and angle of attack from the Pitot tube. Due to uncertainties in the conversion process based on 2D CFD, the absolute value of ~~AoA,~~ the angle of

attack and the consequent absolute Cl ~~, could~~ can not be used for the validation. Therefore, the lift coefficient validation ~~focused~~ focuses on comparing the ~~Cl transients~~ normalized Cl transient responses that are unaffected by the conversion uncertainties. During most of the measurement period, the wind speed was relatively low, between 4 and $6\,\mathrm{m\,s^{-1}}$, keeping the wind turbine close to the minimum operational rotor speed. For the validation, a three-hour time interval characterized by a relatively constant wind (between 4 and $5\,\mathrm{m\,s^{-1}}$ 10 minutes mean wind speed) with low turbulence intensity (below 10%) ~~was~~ is selected from the measurement period. The low variation of mean wind speed and low turbulence intensity ~~were~~ is beneficial in reducing the variability range of the lift coefficient, facilitating the calculation of the average Cl transient curve during flap actuation. In ~~this~~ the selected time interval, the flap was performing on-off actuation cycles, switching between 60 s at ~~full~~ middle-pressure ~~activation~~ actuation and 60 s at ~~complete deactivation, for~~ deactivated state, completing a total of ~~full activation and deactivation~~ 90cycles.

5.2 Aeroelastic simulations

The aerodynamic setup of the BHawC and HAWC2 models is configured as similarly as possible to minimize the differences between the aeroelastic models. Both models have the BEM implemented on a polar grid, as described in Aagaard Madsen et al. (2020), to better account for the rotor induction imbalance due to the flap equipped on only one blade. Furthermore, they implement a potential flow tower shadow model linked to the tower top movements.

The same set of aeroelastic simulations ~~was performed with BHawC and HAWC~~ is performed with the two aeroelastic codes to compute the average Cl transient curve during flap activation and deactivation. The ~~Cl was affected by the variation of the wind field along the rotor plane (due to wind shear or wind veer, for example) and by the rotor tilt and cone angles. The average Cl transient curve was obtained by averaging~~ set consists of 12 simulations with flap actuation ~~occurring at different azimuth angles(FA angle), reducing the Cl azimuthal fluctuation's impact on the transient estimation. Precisely, the set consisted of 12 simulations with FA angles evenly spaced. All simulations were~~ happening at evenly spaced azimuth angles. All simulations are 2 minutes long~~and were run at~~, with a constant wind speed of $5\,\mathrm{m\,s^{-1}}$ ~~,~~without turbulence, ~~at the~~ with standard air pressure ~~, and with~~ and a wind shear of 0.2. The flap ~~started~~ starts in the deactivated position, ~~was~~ is activated at t=30 s, and deactivated after 60 s, at t=90 s, reproducing the activation and deactivation cycles performed on the ~~PT~~Prototype. The flap actuator model of both BHawC and ~~HAWC PT aeroelastic models were~~ HAWC2 Prototype aeroelastic models are updated to match the tuning described in Chapter 4. The Cl ~~was~~ is calculated at the blade section where the pressure measurement system was installed. ~~To minimize the difference between the two aeroelastic models, the aerodynamic setup of the models was configured as similarly as possible. Both models had the BEM implemented on a polar grid, as described in Aagaard Madsen et al. (2020), to better account for the rotor induction imbalance due to the flap equipped on only one blade. Furthermore, they implemented a potential flow tower shadow model linked to the tower top movements.~~

5.3 Average lift coefficient transient response curve on a wind turbine blade section

The rotor cone and tilt angles of the wind turbine, ~~along~~ together with the variations in wind speed resulting from wind shear, veer, and large turbulence structures, contribute to periodic fluctuations in the lift coefficient. These fluctuations ~~challenged~~

challenge the detection and characterization of the ~~transient Cl~~ CL transient response caused by flap actuation. The averaging of cases with flap actuation occurring at different azimuthal positions substantially ~~reduced~~ reduces the azimuth-dependant variation of Cl, with the quality of the average Cl transient ~~quality improved~~ curve improving as the flap actuation azimuthal positions ~~were~~ are more evenly and balanced spread. Ideally, the curve should be obtained by averaging an equal amount of actuation responses starting at every azimuthal angle.

In the case of the aeroelastic simulations, the average Cl transient ~~was~~ curve is derived through the binning (based on the simulation time) of the 12 simulations~~with evenly spaced FA angles. This procedure was performed for both BHawC and HAWC2 simulations.~~ , each with the flap actuation happening at an evenly spaced azimuth angle. Figure 5a shows the Cl time series (dotted lines), normalized to the average Cl increase, from the BHawC simulations around the flap activation time (t=0 s). The azimuth-dependant oscillations of Cl amount to around 40% of the Cl variation due to flap activation (ΔCl_F) and affect the slope and shape of ~~Cl transient~~ the Cl transient curve during the flap activation. Instead, the average ~~Cl transient~~ of the Cl curves (black line) is constant before the activation~~and~~ ; then, it rises at an almost constant rate until it settles to a constant value after approximately 2.5 s. A similar pattern, but with a longer settling time of around 5 s, is exhibited ~~by the averaged Cl transient~~ during flap deactivation, as shown in Figure 5b. The results from the HAWC2 simulations ~~were~~ are almost identical to the BHawC results and are not included in this ~~paper~~ chapter for brevity.

Regarding the measurement data, the times of flap actuation (both activation and deactivation) ~~were~~ are determined by identifying the instant at which the gradient of the flap actuation pressure started to change~~, as the flap valve was located directly at the output of the supply valve~~. Subsequently, the Cl time series ~~were~~ are segmented into temporal windows centered around the flap actuation time and synchronized accordingly. The average Cl transient ~~was~~ curve is finally obtained by binning the Cl signals based on the time window. Different filtering techniques ~~were~~ have been tested to reduce the oscillation of the averaged ~~Cl transient~~ curve caused by turbulence and measurement noise. The best results ~~were~~ are achieved with a low-pass, zero-phase digital filter set to attenuate frequencies above 9P (9 times the rotor rotational frequency) without affecting the slope of the Cl transient. For accurate validation, synchronizing the Cl ~~measurement with the PT measurements was~~ measurements with the Prototype measurements is crucial in ensuring the precise timing of the Cl variation relative to flap actuation pressure. ~~Initially, the synchronization relied~~ The synchronization relies on the GPS time recorded by the flyboard, ~~which was~~ further refined by aligning the time of maximum acceleration along the blade length (also measured on the flyboard) with the time the blade ~~was~~ is oriented toward the ground. ~~During~~ In the average Cl curve calculation, some measurements ~~were~~ are discarded due to insufficient data quality, ~~leading~~ reducing the transient cases to 46 ~~measured transients being used~~ for activation and 63 for deactivation. The measurements ~~had~~ have an acceptable distribution of the ~~flap actuation azimuthal angle~~ azimuthal angle at flap actuation, as shown in Table 1, with three cases or more for all sectors. Figure 5c shows the normalized measured Cl ~~transient~~ curve during flap activation (dotted lines). These ~~transients~~ curves exhibit a higher variability than the aeroelastic ~~simulations~~simulation curves, with a range of the same order of amplitude of the increase in Cl due to flap activation~~, variability mainly caused by the wind turbulence (~~. The wind turbulence is another cause of the measurement's variability, a parameter omitted in the simulations due to the difficulties in estimating the correct ~~value of turbulence for very short simulations)~~turbulence value for a very short simulation time. Nevertheless, the averaged Cl transient curve (black line)

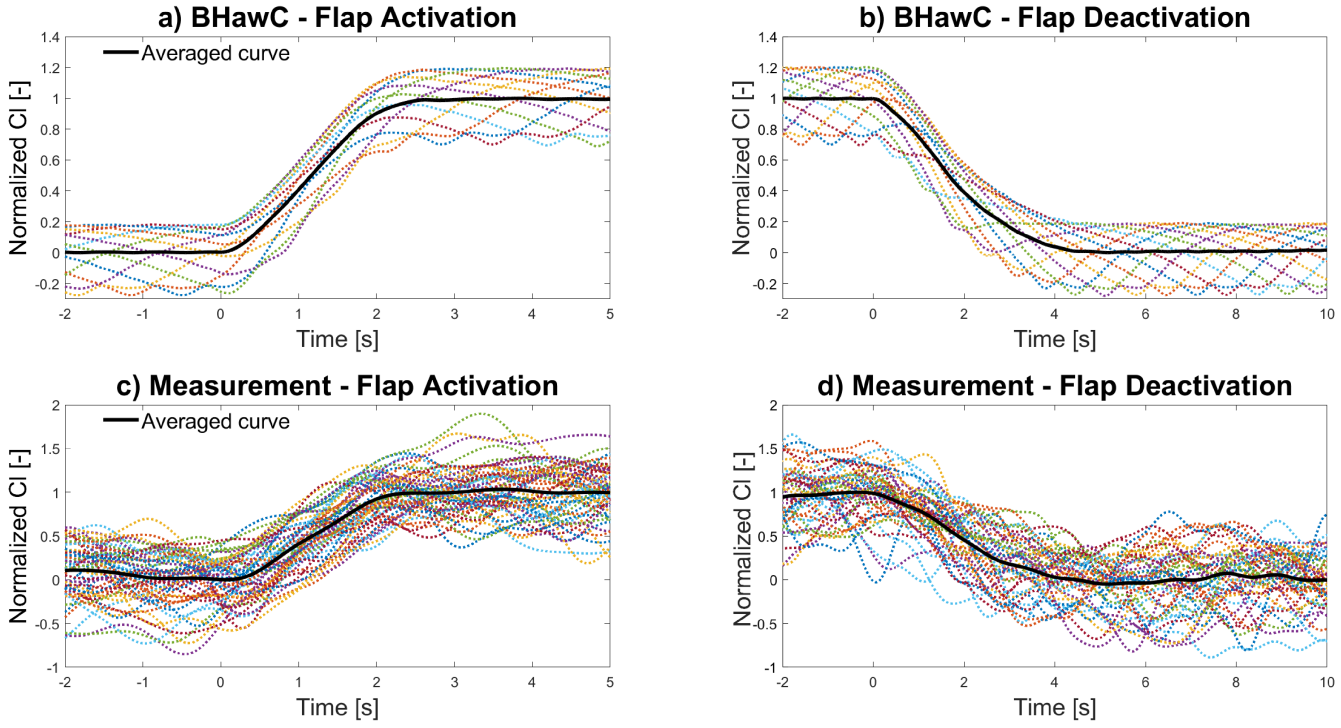

Figure 5. Figures a and b show the normalized averaged Cl transient curve (black line) for flap activation and ~~flap~~ deactivation ~~, respectively,~~ obtained from ~~the~~ averaging ~~of~~ the Cl ~~transient~~ signal of 12 BHawC simulations (dotted lines). Similarly, Figures c and d show the normalized averaged Cl transient curve (black line) ~~, respectively,~~ for flap activation and deactivation ~~,~~ obtained from averaging the measured Cl ~~transient~~ signals (dotted lines).

	Number of measured transients per flap actuation azimuth angle												
	Total	***0***	***30***	***60***	***90***	***120***	***150***	***180***	***210***	***240***	***270***	***300***	***330***
Cl activation	53	4	7	3	3	3	2	5	5	5	2	9	5
Cl deactivation	46	3	3	3	3	4	3	4	6	4	5	4	4
MBr activation	69	6	8	4	4	4	9	5	5	6	3	9	6
MBr deactivation	69	7	5	3	9	5	5	4	5	6	8	6	6

Table 1. Number and azimuth distribution of measured cases used ~~for~~ to calculate the ~~calculation of the~~ average Cl transient and average ~~blade to blade~~ blade-to-blade moment difference (~~MBr~~BMD) during flap activation and deactivation.

exhibits a clear and almost linear variation from a slightly decreasing value before the activation to an almost constant value after the activation. The averaged Cl transient during flap deactivation (black line in Figure 5d) shows a higher fluctuation behavior than the activation transient but is still considerably smoother than the measurements.

5.3.1 ~~Blade-to-blade azimuth based blade root moment~~

5.4 Blade-to-blade azimuth based blade root moment

Another crucial aspect for validating the aeroelastic model of the ATEF ~~was~~ is the analysis of the blade root ~~moment transient~~ bending moment transient response resulting from flap actuation. However, measuring this load transient proved challenging due to its high-frequency response, often hidden within the complex dynamics of the blades responding to factors such as turbulence, shear, vibrations, and rotation. Gomez Gonzalez et al. (2021) introduced a blade-to-blade (b2b) analysis method to compute the load transient response caused by the ATEF actuation. This approach ~~involved~~ involves calculating the difference between the loads acting on the blade with the flap and the load acting on another blade without the flap, but delayed by a time corresponding to a third of one rotor rotation. This artificial time shift ~~aimed~~ aims to synchronize the load time series of blades in the same azimuthal position, thereby mitigating the influence of periodic signal dynamics resulting from rotation, forced vibrations, and wind shear.

This paper proposes a novel azimuth-based b2b method (az-b2b) calculating the load difference by interpolating the loads based on the cumulative azimuth position instead of relying on time shifting. The method comprises three steps. Firstly, the ~~Cumulative Sum~~ cumulative sum of the azimuthal ~~Angle (CSA)~~ angle is calculated for each blade. Secondly, the load of the blades without the flap is interpolated as a function of the ~~CSA of the~~ cumulative sum of the azimuthal angle of the blade with the flap. Lastly, the difference between the load of the blade with the flap and the interpolated load of the blade without the flap is calculated.

Notably, the az-b2b method eliminates the need to initially segment the time series around the relevant event, as the previous b2b method ~~requires. It~~ required, and it can be applied directly to the entire time series in a single run. Additionally, the az-b2b method is not dependent on the calculated mean rotor speed, which is influenced by the time extension of the segments. This characteristic makes it less sensitive to minor variations in rotor speed. By ensuring that the load difference is calculated between two blades positioned at the same azimuthal location, the az-b2b method effectively reduces azimuthal-dependent load fluctuations. However, precise measurement of the azimuthal angle is essential to avoid errors during the interpolation phase. Like the original b2b method, the az-b2b method is still sensitive to high rotor speed variation that can result in a significant variation of data density for azimuthal angle, potentially affecting the quality of the interpolation result.

The az-b2b method ~~was~~ is utilized to calculate the differences in flapwise bending moments at the blade root ~~(MBr1 and MBr2)~~ between the blade with flap ~~(BF)~~ and the remaining blades (~~B1 and B2~~blade 1 and blade 2) in the aeroelastic simulation sets of BHawC and HAWC2. As shown later in this paper, the two blade-to-blade differences ~~did~~ do not differ significantly in both simulations and measurements; therefore, the ~~mean MBr (MBrM)~~ "mean of the two ~~b2b differences was used as reference transient~~azimuth-based blade-to-blade flapwise bending moment differences at the blade roots" (BMD in the remaining part of the paper) is used as a reference channel. Finally, the binning ~~of the twelve simulations~~ (as a function of the simulation time~~computed the average MBrM transient~~) of the twelve simulation signals computes the average BMD transient curve. Figure 6a shows the ~~MBrM transients~~ normalized BMD curves (dotted lines) obtained from the BHawC simulations, together with the ~~average MBrM~~ normalized average BMD transient curve (black line). All the signals ~~were~~ are normalized in order to

make the increase of the b2b moment due to flap actuation unitary. The azimuthal variability of the ~~MBrM transients~~ BMD curves is present but significantly lower than the Cl ~~transients~~curves, being less than 10% of the average transient curve. The average ~~MBrM transient~~ BMD curve is almost constant before the flap actuation, ~~and~~ then it rises smoothly from around 0.5 s until it converges to an almost constant value after 2 s. The average ~~transients~~ curves of the individual b2b differences (~~MBr1 and MBr1 represented by a~~ dotted blue line and ~~a~~ dotted red line~~, respectively~~) exhibit only a ~~small~~ slight difference between themselves. Similar considerations are valid for the ~~MBrM transients~~ BMD curves during flap deactivation shown in Figure 6b. The ~~MBrM transients~~ BMD curves from the HAWC2 simulations were almost identical to the BHawC results and are not included in this ~~paper~~ chapter for brevity.

Regarding the measurement data, the same methodology employed for the Cl transient ~~was~~ is applied to compute the blade load difference. The measurement signals ~~were~~ are segmented into temporal windows centered around the actuation time and synchronized accordingly. Subsequently, the consistency of the azimuthal angle signal ~~was~~ is verified, and the rotor speed ~~was~~ is leveraged to compute the missing or erroneous values. Afterward, the ~~MBrM transients were~~ BMD curves are computed, and the average ~~MBrM was~~ BMD transient curve is obtained using the binning approach. ~~In the average MBrM calculation~~ , The average BMD calculation uses the same number of measured time series (69) ~~were used~~ for flap activation and ~~flap~~ deactivation. The distribution among the rotor sector of the flap actuation azimuthal angle ~~was~~ is also acceptable, with most sectors having at least five cases. Similarly to the results from the Cl ~~transients, the MBrM measured transients~~ transient curves, the BMD measured transient curves (dotted lines in Figure 6c) show a high oscillation, ~~mainly~~ partly caused by the wind turbulence, with a range comparable with the load increase due to the flap activation. Nevertheless, the averaged ~~MBrM transient~~ BMD transient curve (black line) is almost constant before the activation~~and~~ , then smoothly increases and converges to the flap actuation value with minor oscillations. The average ~~MBr1 and MBr2~~ curves of the individual b2b differences are also close to each other, with a ~~max~~ maximum difference of 0.1 normalized BMD. Similar considerations can be done for the flap deactivation case, shown in 6d.

5.5 ~~Validation~~ Initial validation results and discussion

~~In comparing~~ To compare the simulation results with the measurements, the actuation pressure signal ~~was~~ is used to synchronize the ~~transients~~transient curves. In detail, the time the flap pressure gradient undergoes a quick change ~~was~~ is aligned with the flap activation time in the simulations. For the deactivation case, an additional delay of 0.3 s ~~was~~ is added to the simulation flap deactivation time to properly align the simulated Cl and blade-to-blade loads with the measurements. ~~We~~ The authors believe this delay is related to the structure of the pneumatic actuator system, and it would have been identified during the actuator system tuning if the flap state controller signal had been available. For the activation phase, a time delay ~~was~~ is not clearly needed.

~~The~~ Figures 7a compares the simulated and measured Cl ~~transients are compared in Figures 7a~~ transient curves for flap activation and 7b for flap deactivation. In the figures, the synchronized flap actuation time is indicated by the estimated flap ~~command~~ control signal (black dashed line), used in the simulation to actuate the flap, and the measured flap pressure signal (blue dotted line). The ~~transients~~ average Cl curves from BHawC (blue dashed line with x marker) and HAWC2 (red dashed-dotted line)

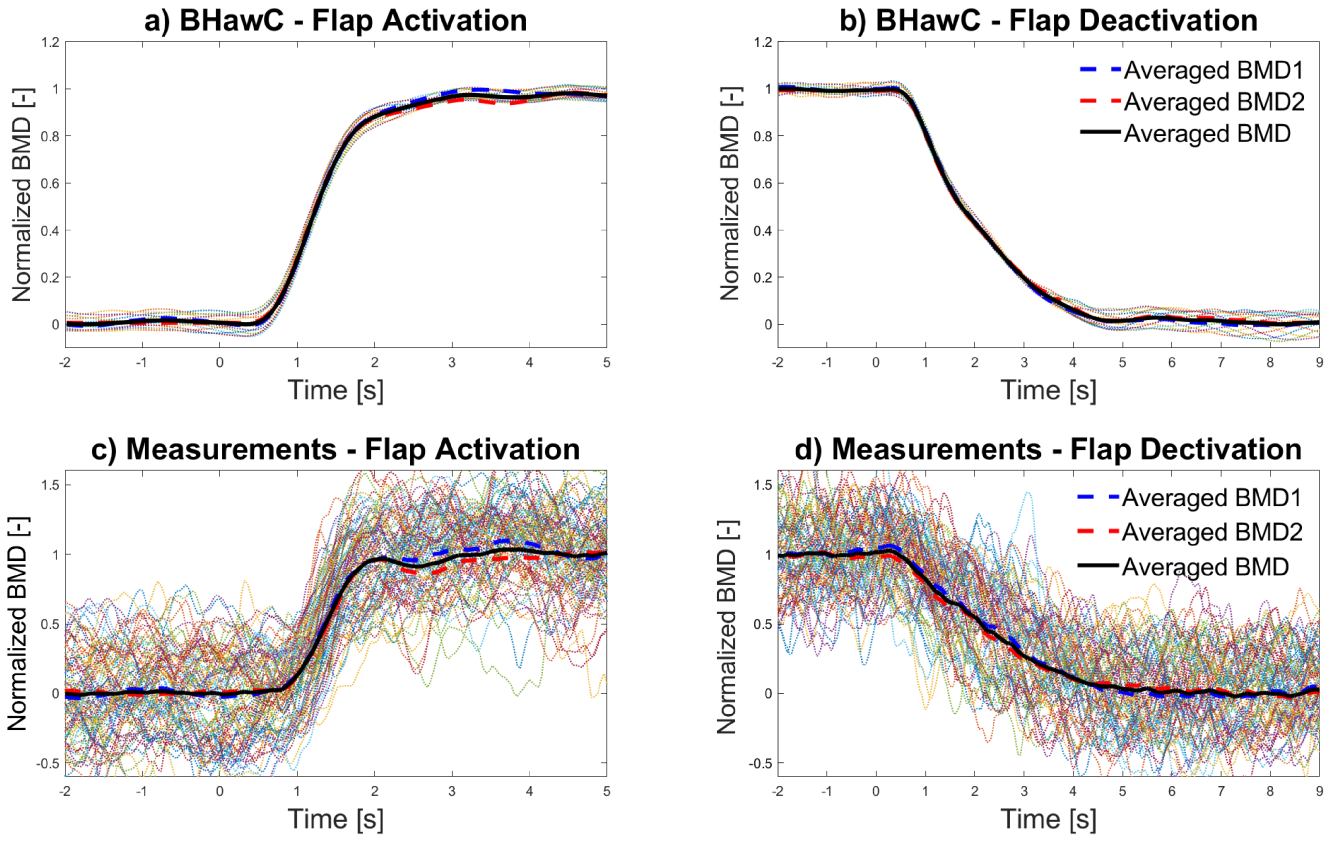

Figure 6. Figure a and b show the normalized averaged b2b bending moment difference at blade root (~~MBrM~~BMD) transient curve (black line) for flap activation and flap deactivation~~respectively~~, obtained from the averaging of the ~~MBrM transient~~ BMD signals of 12 BHawC simulations (dotted lines). Similarly~~Figure~~ , Figures c and d show the averaged normalized ~~MBrM~~ BMD transient curve (black line) for flap activation and deactivation~~respectively~~, obtained from ~~the~~ averaging ~~of~~ the measured ~~MBrM transient~~BMD signals (dotted lines). All the plots also include the b2b bending moment difference between the blade with flap and ~~the blades without~~ blade 1 (~~MBr1~~BMD1: dashed blue line~~, MBr2~~) and blade 2 (BMD2: dashed red line)

simulations closely match each other, with a maximum difference below 6% of the ΔCl generated by the flap actuation in both flap activation and deactivation cases, mainly caused by an offset of ~~a single time step~~ two time steps (0.04 s) between the two transients. The simulated ~~Cl has transients~~ average Cl curves are significantly similar to the measurements (black line with round markers). In the activation case, the maximum difference is below 40% of the measurements std, below 8% of the ΔCl, with the simulated Cl curves starting to increase 0.1 s (5% of the time for full flap activation) before the measurement ~~Cl~~ curves but at a lower slope, and ~~it converges~~ they converge to full activation with a delay of 0.15 s (7.5% of the ~~full~~ complete flap activation time). In ~~the~~ deactivation, the maximum difference is below 6% of the measurements std, below 8% of the ΔCl~~, and the simulated Cl starts~~ . The simulated Cl curves start to decrease with a delay of 0.2 s (4% of the full flap deactivation time)

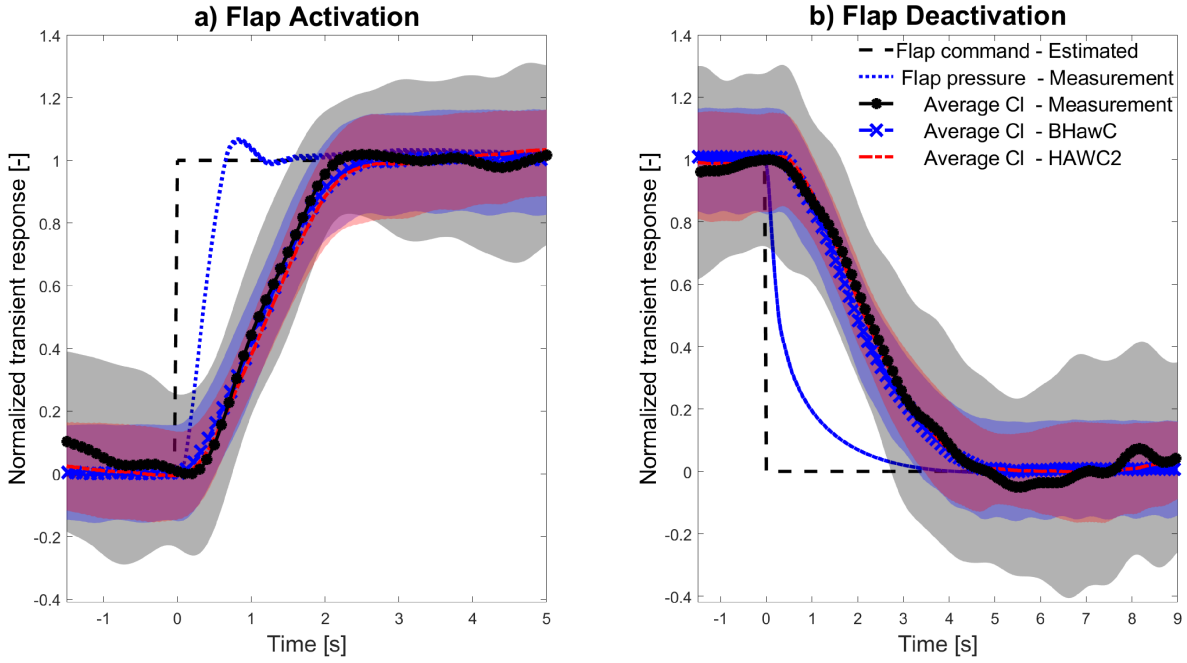

Figure 7. Comparison of the normalized averaged Cl transient curves obtained from BHawC (blue dashed line with x marker) and HAWC2 (red dash-dotted line) simulations and measurements (black line with asterisk marker) during flap activation (a) and deactivation (b), including an error band of ~~1~~ one std of the matching colors. The normalized measured flap pressure (blue dotted line) and the estimated flap ~~command~~ control signal (black dashed line) are also included.

that quickly recovers~~, and afterward it precedes the measurement slope~~. Afterward, they precede the measurement curve of less than 0.1 s (2% of the full flap deactivation time) until full deactivation. The std of the simulated ~~transients~~ curves are often equivalent~~, and~~. They are nearly half of the measurement std~~. This difference is~~, mainly due to the omission of turbulence in the aeroelastic simulations.

The b2b moment ~~transients~~ transient curves are compared in Figures 8a for flap activation and 8b for flap deactivation. Similarly to the Cl comparison, the ~~MBrM transients~~ average BMD transient curves from BHawC (blue dashed line with x marker) and HAWC2 (red dashed-dotted line) simulations closely match each other, with a maximum difference below 7% of the Δ~~MBrM~~ BMD due to the flap actuation in both flap activation and deactivation cases, mainly caused by an offset of 0.06 s between the two ~~transients. Both transients~~ curves. Both curves have a std significantly smaller compared to the Cl ~~transients~~curves, showing the benefit of the az-b2b method in removing the impact of the azimuthal load oscillations. The HAWC2 ~~transient having~~ curve shows a std almost twice ~~the std~~ that of the BHawC simulations~~is mainly related to higher rotor speed oscillations caused by a not perfect~~. The main reason is a higher oscillation in the rotor speed originating from an imperfect implementation of the SGRE controller in the HAWC2 code. The simulated ~~MBrM has transients~~ average BMD curves are similar to the measurements (black line with round markers). In the activation case, the maximum difference is below 55% of the measured std and

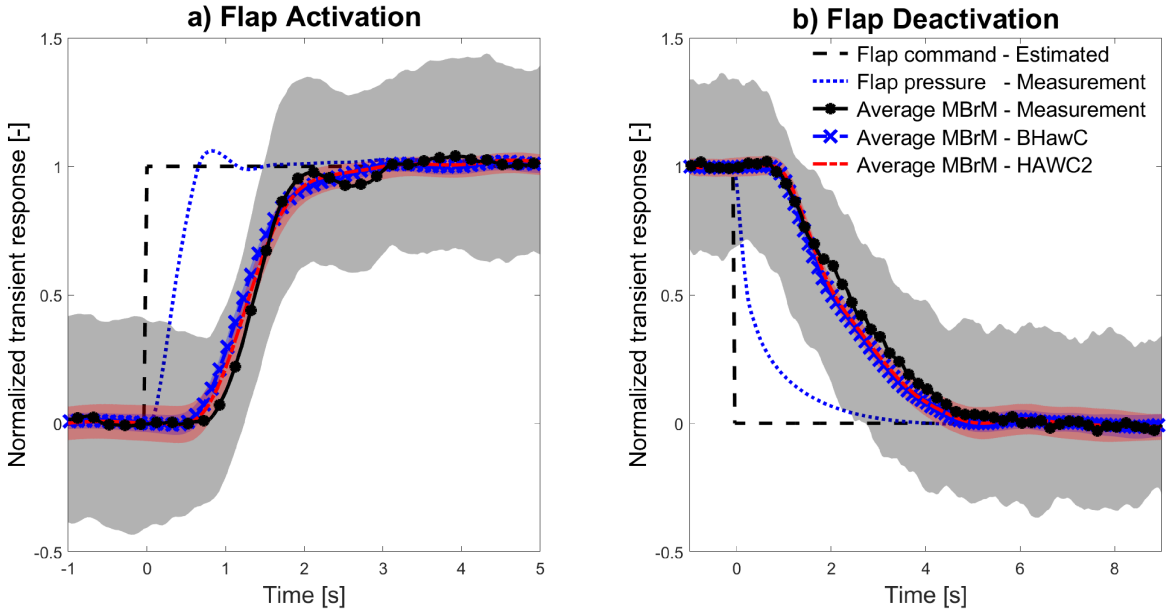

Figure 8. Comparison of the normalized averaged b2b blade root bending moment (~~MBrM~~BMD) transient curves obtained from BHawC (blue dashed line with x marker) and HAWC2 (red dash-dotted line) simulations and measurements (black line with asterisk marker) during flap activation (a) and deactivation (b), including an error band of ~~1~~ one std of the matching colors. The normalized measured flap pressure (blue dotted line) and the estimated flap ~~command~~ control signal (black dashed line) are also included.)

17% of the Δ~~MBrM~~ BMD due to the flap activation. Mirroring the Cl ~~transients~~transient curves, the simulated ~~MBrM~~ BMD begins to increase 0.2 s (10% of the ~~full~~ complete flap activation time) before the measured ~~MBrM~~ BMD but at a lower slope, and it converges to full activation within the measurement fluctuation transient. In the deactivation, the maximum difference is below 60% of the measured std, below 20% of the Δ~~MBrM, and the simulated Cl starts~~ BMD. The simulated Cl curves start to decrease with a delay of 0.2 s (5% of the ~~full~~ complete flap deactivation time) that ~~quickly recovers and afterward precedes~~ is quickly recovered. Afterward, they precede the measurement slope of less than 0.1 s until ~~full~~ complete deactivation.

Another purpose of the initial validation ~~was~~ is tuning the ATEF model to ensure the proper synchronization between the simulated and measured Cl and ~~MBrM transients~~BMD transient curves. Figure 9a shows all the ~~ATEF aeroelastic model~~ signals relevant for the ATEF aeroelastic model tuning during flap activation. The ~~measured~~ flap state controller signal was not recorded in the measurement campaign. Therefore, the measured flap pressure (blue dotted line) synchronizes the simulated flap control signal (black dotted line). This control signal commands the flap deflection (red dashed line with circular markers), deflection obtained from the post-processing of the flap deflection videos (green squared markers). The Cl transient follows the flap deflection by a few milliseconds in the simulations (blue line with squares and orange line) and by 0.1 s in the measurements (grey line with arrow marker). The slight difference between the simulated and measured Cl transients (especially if compared to the measurements std) confirms the current model (with ~~the~~ a linear relation between flap deflection and Cl

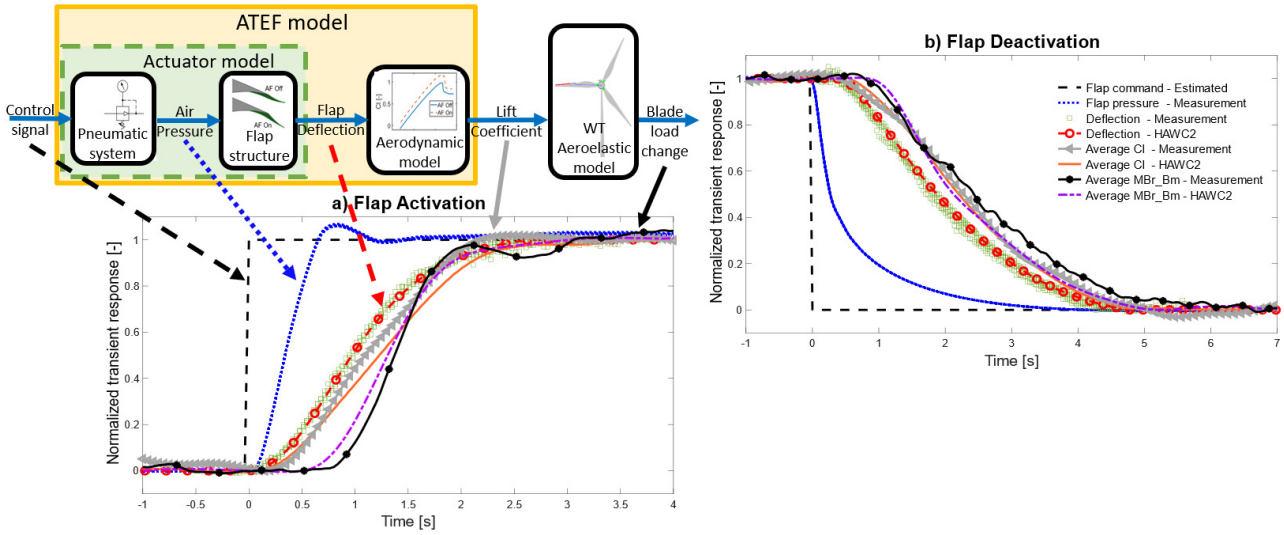

Figure 9. a) Signals relevant for ~~the~~ modeling and ~~validation of~~ validating the flap model during flap activation ~~,~~ linked to the ATEF model scheme. ~~Transients of Flap~~ Estimated flap state controller ~~command~~ (black dashed line), normalized flap pressure (blue dotted line), measured and ~~estimated~~ simulated flap deflection (green squares and red dashed line with circles), measured and ~~estimated~~ simulated Cl curves (gray line with triangle and red line) and measured and ~~estimated MBrM~~ simulated BMD curves (black line with asterisks and ~~reddash-dotted~~ violet dash-dotted line) are plotted to verify the time tuning of the aeroelastic model. b) Signals relevant for the modeling and validation of the flap model during flap deactivation

variation) provides reliable results. ~~After~~ The simulated BMD curve rises 0.5 s after the Cl increase, ~~the MBrM transient starts 0.later, with the simulations anticipating the measurements of~~ anticipating the measured curve by 0.2 s. Figure 9b shows the signals relevant for the ATEF model tuning during flap deactivation. To properly align the ~~simulations Cl and MBrM transients~~ simulated Cl and BMD curves with the measurements, a delay of 0.3 s ~~was~~ is introduced in the actuator model between the flap state controller and the flap deflection during deactivation only.

In conclusion, the initial validation showed a good agreement between the simulated and measured ~~Cl and MBrM transients~~average Cl and BMD transient curves. However, small differences in the ~~transients motivated~~ curves motivates the broader validation described in the following section.

6 Extended ATEF ~~Aerodynamic~~ aerodynamic model validation

The validation of the ~~aerodynamic model of ATEF aeroelastic was~~ ATEF aerodynamic models is extended to a wider range of environmental conditions with the measurements obtained ~~with the PT field campaign~~ from the Prototype field campaign run between October and December ~~2020, when the ATEF system was tested for different pressure activation and activation patterns. In this~~ 2020. In this part of the test campaign, the flyboard was not present, and the validation ~~did not rely on the Cl measurements but~~ can rely only upon comparing the transient of the blade-to-blade moment at the blade root ~~(MBrM)~~ during

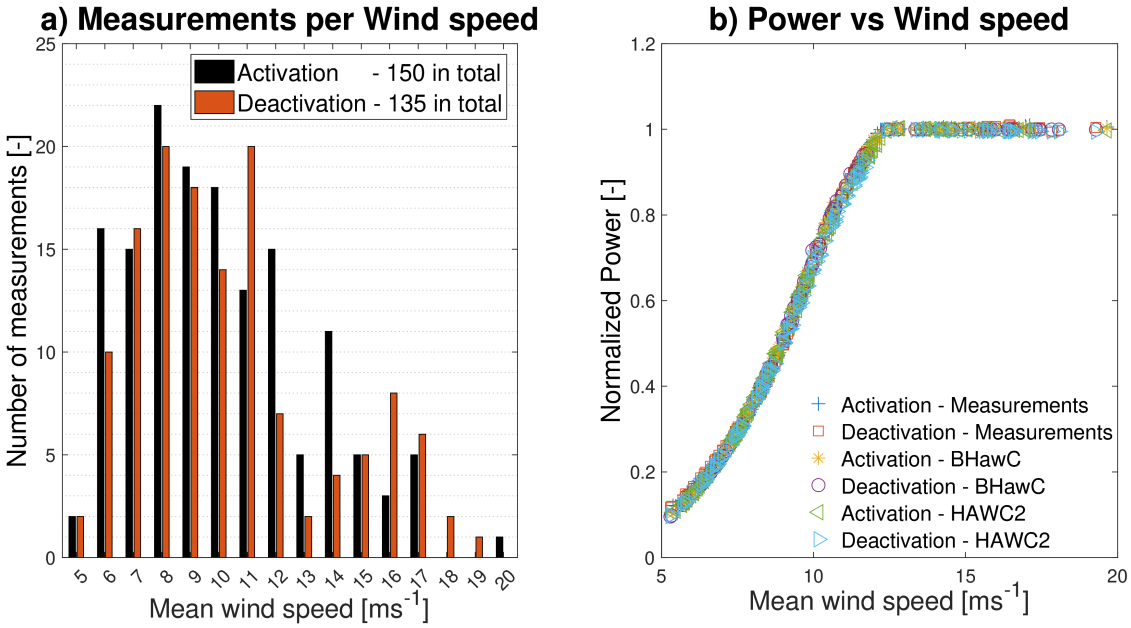

Figure 10. a) Number of selected measurements per wind speed for flap activation (black) and deactivation (red). b) Normalized power curve of the selected measurements and ~~simulation~~ simulations (~~both~~ BHawC and HAWC2) for flap activation and deactivation.

flap activation and deactivation. The validation ~~followed~~ follows the so-called one-to-one ~~(o2o)~~ approach, where the measurements are compared with a set of simulations reproducing the ~~WT~~ wind turbine operating under the same environmental conditions measured at the time of the flap actuation. As the validation ~~focused~~ focuses on the short transient happening within 10 s after the flap activation and deactivation, the simulations ~~did not rely on the 10 minutes~~ rely not on the 10-minute averaged environmental condition but on the actual condition measured at the flap actuation time.

6.1 Field campaign

Between October and December 2020, the ATEF system on the ~~PT~~ Prototype was tested for several actuation pressure and activation ~~pattern~~patterns. The measurements of full activation and deactivation cycles at middle ~~activation~~ actuation pressure with the ~~WT~~ Prototype operating in normal production ~~were~~ are selected for validation. Additional filtering ~~removed~~ removes the measurements at which the wake of the ~~PT~~ Prototype or the nearby ~~WTs~~ wind turbines affected the met mast measurements. As a change in the ~~WT~~ wind turbine operative condition could result in ~~an MBrM variation interfering~~ a BMD variation and interfere with the load transient response due to flap actuation, only flap actuation ~~cases~~ occurring when the ~~WT~~ Prototype was in almost stationary condition ~~were~~ is selected. This selection ~~was~~ is achieved by removing the cases where, within 10 s before and after the flap actuation, the pitch angle varied more than 1 deg, the rotor speed more than 0.5 rpm, and the yaw direction more than 1 deg. Finally, a total of 150 measurements for flap activation and 135 for flap deactivation ~~were~~ are obtained, dis-

tributed between 5 and 20 ms^{-1} as shown in Figure 10a.

6.2 Models and simulations setup

The BHawC and HAWC2 models from the initial validation described in section 5 ~~were~~ is used for this validation, including the additional $0.3\,\mathrm{s}$ deactivation delay in the flap actuator model.

To properly calculate the b2b load transient curve during flap actuation, the simulation setup ~~had~~ has to match the environmental conditions at the ~~WT~~ wind turbine at the specific time of the flap actuation. The environmental conditions were measured at the met mast, located $300\,\mathrm{m}$ in front of the ~~PT~~Prototype. This distance introduced a time delay ~~Td~~ T_d corresponding to the time the wind needs to cover the distance ~~Dm~~ D_m between the met mast, where it was measured, and the ~~WT~~ wind turbine rotor. This delay is inversely proportional to the wind speed (~~Td~~T_d=60 s for a low $5\,\mathrm{ms}^{-1}$ wind speed and ~~Td~~T_d=15 s for $20\,\mathrm{ms}^{-1}$ wind)~~and for~~. For a discrete and constant sampling time ΔT ~~was calculated as~~, T_d is calculated as

$$Td T_d = k * \Delta T$$

where k is the first time step, previous of the flap actuation time t_0, for which the sum of the distances traveled by the sampled wind speeds $w_{(-i)}$ covers the distance ~~$Dm.$~~ D_m:

$$k = \min(i \in Z^+ | \sum_{i=0}^{k} w_{(-i)} * \Delta T \geq Dm D_m)$$

The flap actuation time t_0 ~~was~~ is identified by using the flap actuation pressure gradient, as described in section 5. A $20\,\mathrm{s}$ time interval centered on the actuation time, corrected by the corresponding ~~Td, was~~ T_d, is selected for each flap actuation. For each time interval, the mean values of air density, wind shear, and the misalignment angle between the wind direction and the ~~WT yaw angle were~~ wind turbine yaw angle are input to the aeroelastic simulations. As for the simulated wind speed, the effective wind speed value ~~was~~ is preferred to the measured wind speed. The effective wind speed is the wind speed that makes the ~~WT~~ wind turbine operate at the measured rotor speed, generator power, and pitch angle. This wind speed ~~was~~ is obtained by interpolating the measured characteristic power, pitch, and rotor speed curves at the corresponding mean values measured in the selected time interval. The ~~MBrM transient~~ BMD transient curve comparison in section 5 shows ~~the~~ that turbulence has a small impact on the average load transient ~~due~~ response to flap actuation. ~~This average~~ The average BMD curve is instead affected by the ~~distribution of~~ input data distribution among the azimuthal angle at which the flap actuation happens. These conclusions supported the decision to omit the turbulence in the current validation, avoiding the additional complexity of measuring and modeling the equivalent turbulence. At the same time, in the simulations, the flap ~~was~~ is actuated at the ~~corresponding measured FA angle~~ same azimuthal angle that was actuated in the field. Figure 11 shows the distribution of ~~Air~~ air density (a), ~~Wind~~ wind shear (b), ~~Yaw~~ yaw misalignment angle (c), and ~~FA angle~~ azimuthal angle at flap actuation (d) in the function of the effective wind speed used in the simulations. Figure 10b shows the mean power obtained in the simulations ~~matches~~ matching the measured one for all the flap actuation cases.

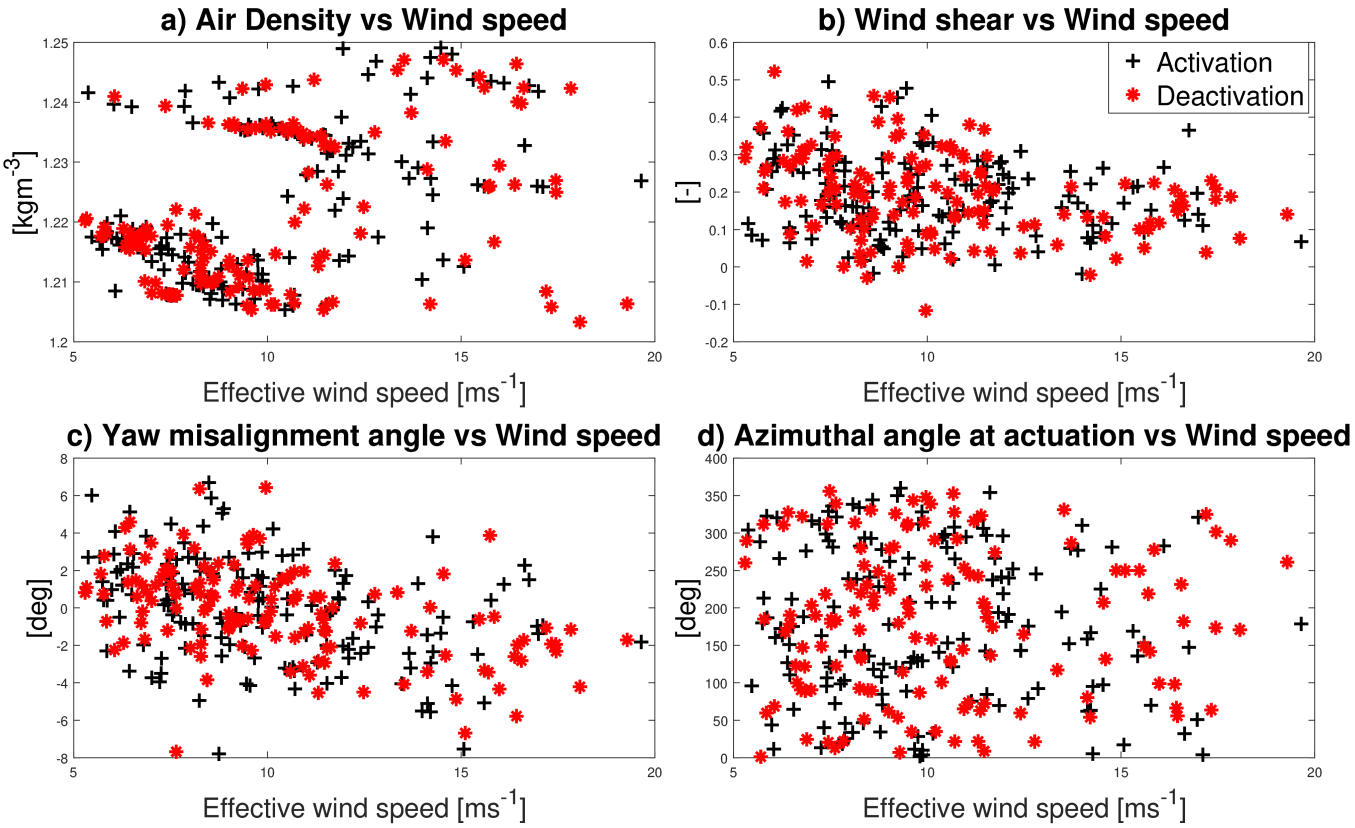

Figure 11. Distribution of ~~Air~~ air density (a), ~~Wind~~ wind shear (b), ~~Yaw~~ yaw misalignment angle (c) and azimuthal angle at flap actuation (d) in function of the effective wind speed used for the flap activation (black cross) and deactivation (red asterisk marker) aeroelastic simulations.

6.3 Extended Validation results

The extended validation of the ATEF aerodynamic ~~model relied~~ models relies on the comparison of the average ~~MBrM transients. The MBrM signal was~~ BMD transient curves. The measured and simulated BMD curves are calculated and synchronized ~~for measurements and simulations~~ as described in section 5.

Figure 12a shows the comparison of the average ~~MBrM transient~~ BMD transient curve during flap activation of the measurements (black line with asterisk marker), ~~BHAwC~~ BHawC simulations (blue dashed line) and HAWC2 simulations (red dash-dotted line) based on all the available data. The simulation ~~transients~~ curves are almost equivalent, with a maximum time shift within 0.6 s (less than ~~3~~ three time steps), ~~bringing the~~ keeping the maximum load difference within 5% of the ΔBMD. The transient ~~pattern also differs from the transient~~ curves also differ from the curves obtained in the initial validation. The load keeps increasing and fluctuates after the flap's full activation, a behavior also shown by the measurement transient. This behavior is probably caused by ~~the averaging of~~ averaging the load difference obtained from all the different wind conditions. The simulation ~~transients~~ curves are well within the error band of measurement transient, with a maximum difference below

50% of the measured std ~~,~~and below 10% of the Δ~~MBrM~~ BMD due to the flap activation. Similarly to the initial validation, the simulation ~~transients~~ curves start to increase earlier (around $0.1\,\mathrm{s}$, 5% of the actuation time of $2\,\mathrm{s}$) but with a lower slope, under-predicting the load increase in the second half of the flap activation and accumulating a delay of $0.2\,\mathrm{s}$, 10% of the actuation time) and then converging within the measured oscillating transient curve. As observed in the initial validation, the simulations cannot reproduce the s-shaped behavior the measurements manifest.

Figure 12b compares the average ~~MBrM transients~~ BMD transient curves during flap deactivation. The ~~simulations transients~~ simulation curves differ less than 3% of the ΔBMD, with a maximum time shift within $0.08\,\mathrm{s}$ (~~2~~ 4 time steps). The simulation ~~transients~~ curves are well within the measured error band, with a maximum difference below 60% of the measured std ~~,~~and below 15% of the Δ~~MBrM~~BMD. The simulation transient decreases $0.2\,\mathrm{s}$ (4% of the $4.5\,\mathrm{s}$ deactivation time) later than the measured ~~transient~~curve, but they quickly converge within the measurement oscillation ~~transient~~curve.

During the actuator model tuning, the flap displays a slower activation and a faster deactivation when the ~~WT~~ wind turbine is in normal operation compared to the idling state. This behavior suggests that the aerodynamic loading on the blade section may influence the deflection of the flap. To investigate this hypothesis, the averaged ~~MBrM transients were~~ BMD transient curves are computed for wind speed ~~ranges of~~ intervals with $2\,\mathrm{m\,s^{-1}}$ range, a wind ~~range with~~ interval with expected similar aerodynamic load values. The averaged ~~transients~~ transient curves are shown in Figure 13 for flap activation and Figure 13 for flap deactivation. For wind speed ~~ranges~~ intervals up to $13\,\mathrm{m\,s^{-1}}$, the simulated ~~transients~~ transient curves closely resembled the corresponding measured ~~transients~~curves, exhibiting differences similar to those observed in the global ~~transients. For the range~~ transient curves. The data is scarce for the intervals above $13\,\mathrm{m\,s^{-1}}$, ~~insufficient data results~~ resulting in irregular and oscillating ~~transients~~transient curves. From the comparison of the measured averaged ~~trends~~ curves shown in figure 15a for flap activation and 15b for flap deactivation, a correlation between the wind speed and the transient ~~shape~~ curve does not emerge clearly. The measured transients all lie within a range of $0.2\,\mathrm{s}$ in both the activation and deactivation phases without a clear relation to the aerodynamic ~~load~~loads.

7 Near Wake model study

In the ATEF model validations described in the previous sections, as well as in the stationary validation of the same ATEF models described in Gamberini et al. (2022), the aeroelastic codes did not model the 3D effects originated by the vorticity trailed from the edges and along the span of the flap section. HAWC2 code can account for these 3D effects via the optional Near-Wake induction model at the cost of higher model and computational complexity. This model, introduced by Pirrung et al. (2017), is a simplified version of the lifting line model specifically designed to examine the wake near each blade. The Near-Wake model ~~, being fully dynamic,~~ accounts for the temporal evolution of the trailed vorticity. The vorticity is traced between all the aerodynamic sections on the blade, allowing the model to capture various vortices, such as tip and root vortices. Furthermore, the model ~~takes into consideration~~ considers vorticity trailed at the edges of flaps and vorticity resulting from radial load fluctuations in turbulent inflow. The strength of the trailed vortex at each trailing point is determined by computing the disparity in bound vorticity between adjacent aerodynamic blade sections. This calculation incorporates an approximation

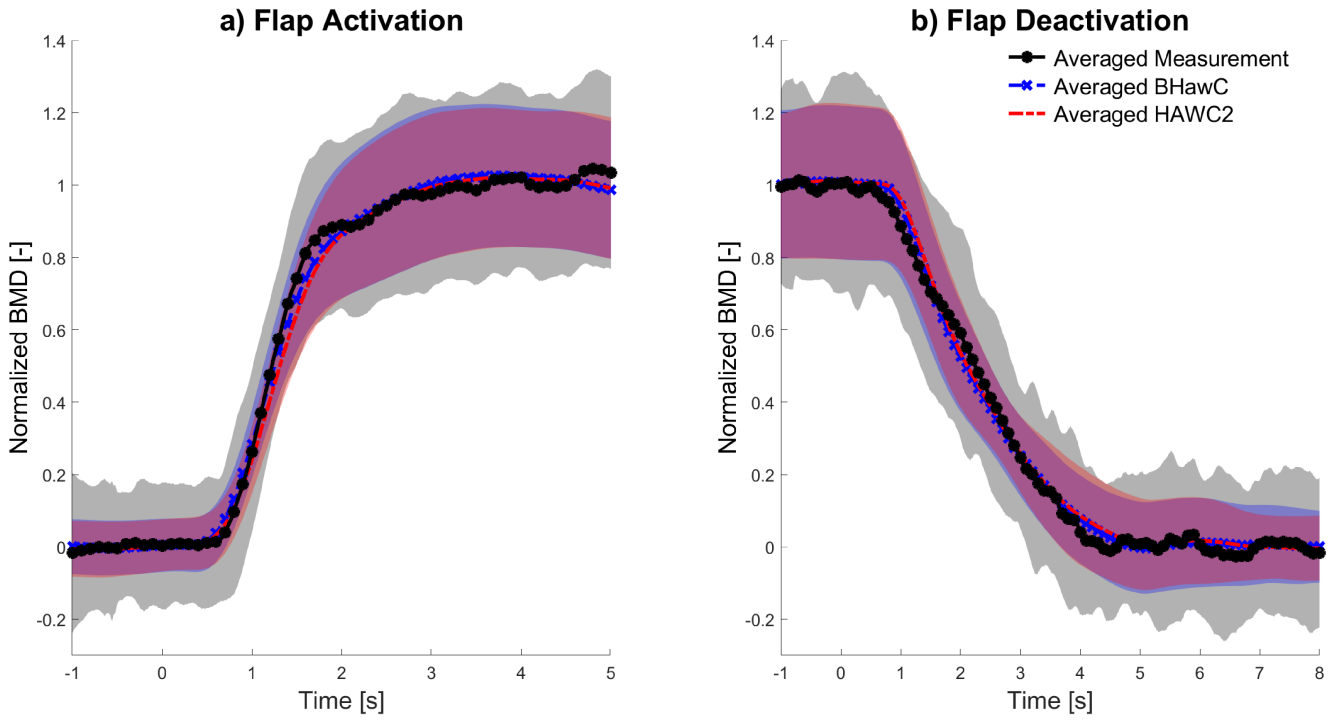

Figure 12. Comparison of the normalized averaged b2b blade root bending moment (~~MBrM~~BMD) transient curve obtained from all BHawC (blue dashed line with x marker) and HAWC2 (red dash-dotted line) simulations and all measurements (black line with asterisk marker) during flap activation (a) and deactivation (b), including an error band of ~~1~~ one std of the matching colors.

of the buildup of unsteady circulation.~~The validation of the WT section properties and the extended validation were performed~~

Prospathopoulos et al. (2021) showed that the Near-Wake induction model improves the prediction of the flap's local and global impact on the thrust forces. These changes in flap performance are investigated by performing the initial and extended validations also with the Near-Wake model ~~active in the~~ enabled in HAWC2 ~~simulations (H2-NW~~(HAWC2-NW). The Near Wake model impacts the ΔCl at the analyzed flap location, reducing the increase of Cl during flap actuation of 7% compared to the HAWC2 results without the Near Wake model~~(H2)~~. The averaged Cl ~~transients~~ transient curves differ less than 3% of the ΔCl during flap activation, mainly due to a time shift of almost ~~2~~ two time steps, and less than 4% ΔCl (time shift around ~~3 time step~~three time steps) during flap deactivation. ~~Regarding the MBrM, the H2-NW transient~~ The Near-Wake model reduces the ΔBMD of the flap actuation between 2 and 2.5%. Meanwhile, the HAWC2-NW BMD transient curve is almost equivalent to the ~~H2 transient~~HAWC2 curve, with a difference below 1% of the ΔBMD during flap activation and below 0.6% ΔBMD during flap deactivation. ~~Additionaly, the Near-Wake model impacts the ΔMBrM of the flap actuation between 2 to 2.5%.~~

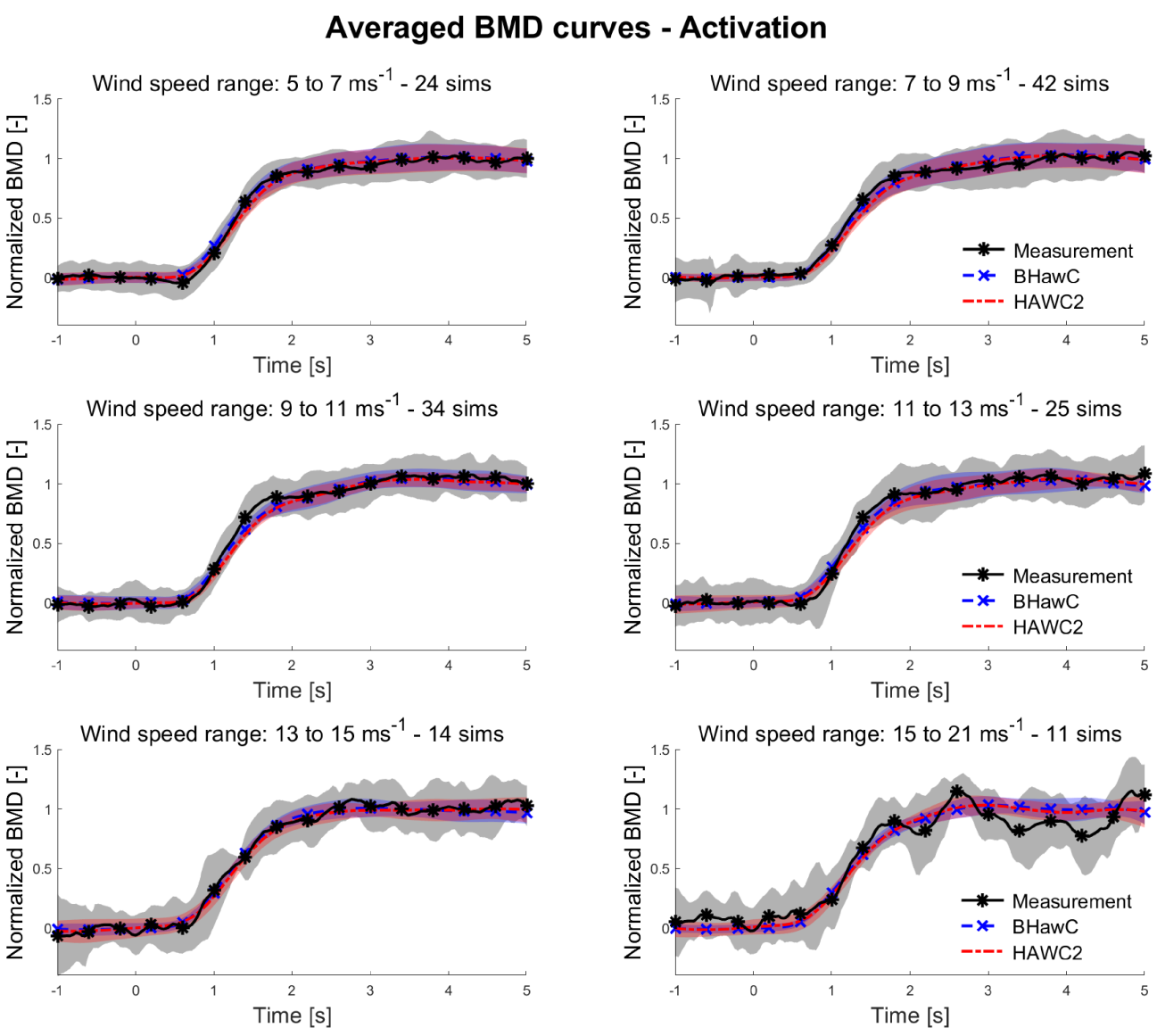

Figure 13. BHawC (blue dashed line with x marker), HAWC2 (red dash-dotted line), and measurements (black line with asterisk marker) averaged ~~MBrM transients~~ BMD transient curves obtained for wind speed intervals of $2\,\mathrm{m\,s^{-1}}$ during flap activation. The number of ~~data-point~~ data points (sims) per wind interval is also specified.

8 General discussion

585 The validations described in sections 5 and 6 show the HAWC2 and BHawC aeroelastic models of the ATEF implemented on the ~~PT~~ Prototype provide almost equivalent results during the flap activation and deactivation. In the initial validation based on

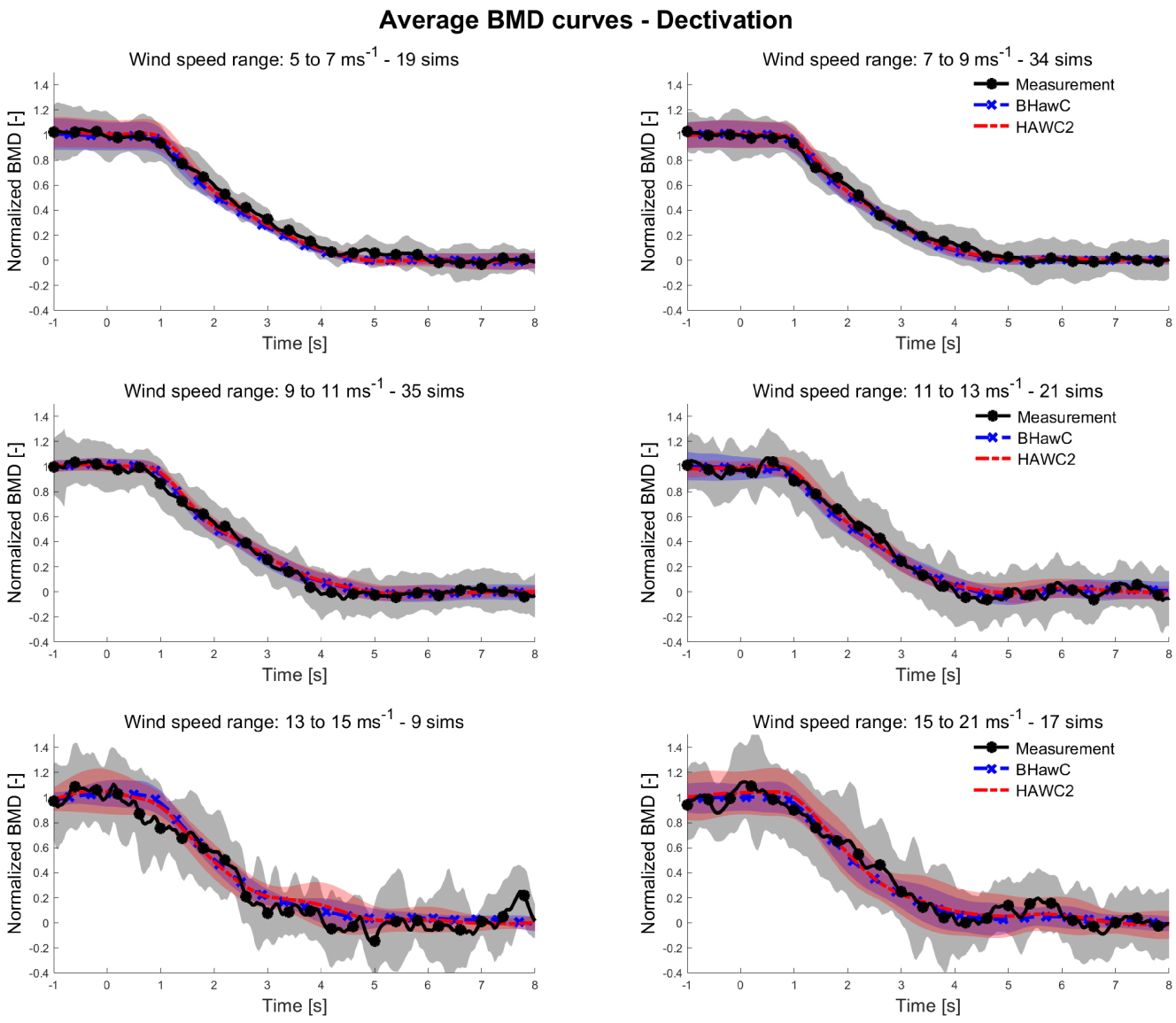

Figure 14. BHawC (blue dashed line with x marker), HAWC2 (red dash-dotted line), and measurements (black line with asterisk marker) averaged ~~MBrM transients~~ BMD transient curves obtained for wind speed intervals of $2\,\mathrm{m\,s^{-1}}$ during flap deactivation. The number of ~~data point~~ data points (sims) per wind interval is also specified.

the blade section measurements, the respective HAWC2 and BHawC Cl transients have a time shift below $0.04\,\mathrm{s}$, leading to a maximum difference lower than 6% of the ΔCl occurring during flap actuation. In the extended validation, the simulated b2b load transients differ less than 5% of the Δ~~MBrM~~ BMD caused by the flap actuation, with the difference mainly originating by a maximum time shift of $0.1\,\mathrm{s}$.

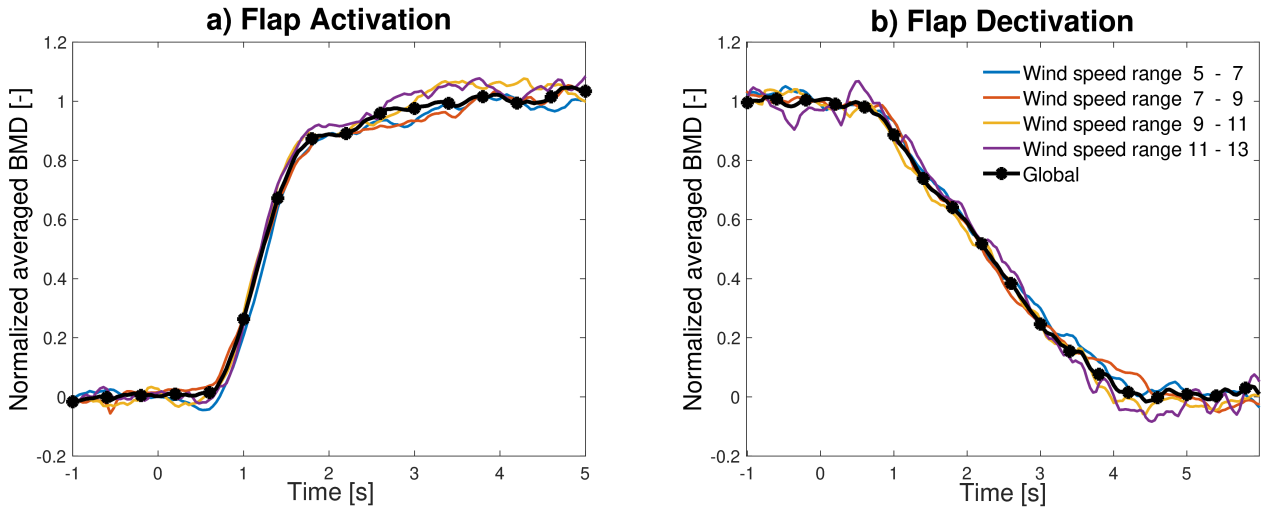

Figure 15. Comparison of the measured ~~MBrM transients~~ BMD transient curves obtained for different wind speed intervals for flap activation (a) and flap deactivation (b).

The validations proved that the simulations are in good agreement with the measurements. The simulated average Cl ~~transients~~ transient curves are well within the error band of the measured ~~transient~~curves, with a ~~max~~ maximum difference below 8% of the ΔCl during flap activation and deactivation. The differences between the simulated and ~~the measured average MBrM transients~~ measured average BMD transient curves are below 10% ~~of the ΔMBrM during flap activation and below 15% during flap deactivation. The ΔMBrM due to flap activation ranges between 6% (at rated wind speed) to 11% (at high or low wind speed) of the mean blade loads (as showed in Figure 4b of Gamberini et al. (2022)). Consequently, the maximum simulation transient error is below 1% of the mean blade load during activation and below 1.7% during flap deactivation.~~ Within this error margin, the simulations cannot completely reproduce the average transients' shape, especially during the flap actuation, where the measurements rise later but steeply, reaching full activation value earlier. The main proposed causes of this difference in the transient shape are:

- Incomplete flap deflection model. The actuator model ~~was~~ is tuned with the flap deflections measured only at one wind speed. The flap deflection transients may vary as the external conditions, like ~~the~~ aerodynamic forces or the rotational speed, change. As shown in Figure 15, ~~comparing MBrM transients at~~ there is no clear correlation between the BMD transient curves from different wind speed intervals ~~does not correlate clearly with the WT operative condition~~and the wind conditions. However, ~~it still has a range of uncertainty~~ the differences between the averaged curves have a magnitude comparable to the ~~differences~~ validation error margin, suggesting that the variation of the external conditions can partly justify the differences observed between simulations and measurements. Furthermore, the ~~tuning flap deflections were~~ flap deflection data was measured only at one blade section, not ensuring the flap has a constant deflection ~~characteristic~~ along its whole 20 m length. A spanwise variation of the flap deflection could justify the steeper shape

of the ~~MBrM~~ BMD transient. Additional measurements of the flap deflection at different blade locations, wind speeds, and ~~WT~~ wind turbine operative conditions can improve the deflection model, reducing the transient shape difference.

- ~~Imperfect~~ Accuracy of aerodynamic properties ~~of the~~ for airfoils including flap~~profiles~~. The Cl and Cd curves used in the aeroelastic simulations were all derived from the wind tunnel measurement of the 21% thickness ~~profile~~airfoil. New wind tunnel measurements for the 18% and 24% ~~profiles and for~~ airfoils and different relative sizes of flap and chord can verify if the flap ~~profiles~~airfoils' aerodynamic properties are correct or responsible for the observed difference in the ~~transients~~transient curves' shape.

- Uneven distribution of the azimuthal angle at flap actuation time in the measurements. The Cl and ~~MBrM~~ BMD transient are strongly affected by the azimuthal angle at which the flap actuation is initiated, as shown in section 5. In the available measurements, the ~~FA angle of the measured flap activation and deactivation~~ azimuthal angle at flap actuation was not evenly distributed on the whole rotor, leading to a distorted averaged transient. In the ~~o2o~~ one-to-one process, this was partly compensated by simulating the flap activation at the measured ~~FA~~azimuthal angle at flap actuation. Additional measurements aiming to ~~improve the FA angle distribution at different~~ balance the distribution of this angle at all wind speeds can potentially improve the quality of the measured ~~transients~~ transient curves and reduce the difference between measurement and simulation.

- Incomplete flap aerodynamic model. The transient ~~shape~~ curve difference can suggest a delay of the change in aerodynamic flow compared to the flap actuation, a delay dependent on the flap position (as it is not present during flap deactivation) that is quickly recovered during the activation. CFD simulations modeling the exact geometry of the flap deflection ~~transient~~ can verify this hypothesis.

Based on the experience gained in the validations presented in this paper, some recommendations are suggested to improve future validation campaigns of ~~ATEF~~active flaps:

- The correct estimation of the flap deflection is crucial in the validation of the aerodynamic model of the ATEF. If continuous measurements of the flap position are ~~not available, the flap deflection transient~~ unavailable, the deflection curve should be measured for several wind and operative conditions to ensure the correct tuning of the actuator model.

- Uncertainties ~~on~~ about the aerodynamic properties of the flap ~~profiles~~ airfoils reduce the accuracy at which the aerodynamic model can be validated. Proper measurements of all the relevant flap ~~profiles~~ airfoils should be conducted. If that is not possible, the Cl and Cd impact of the flap can be derived from similar ~~profiles~~ airfoils with acceptable accuracy.

- The correct time synchronization of all the different measurement systems is crucial to ensure the proper time precision in measuring and validating the transient curves of the Cl and ~~Load channels~~load signals. Therefore, the flap actuator control (or any other channel that can be used to estimate the flap actuation time) is required.

- The azimuthal angle at which the flap is actuated strongly affects the transient curve of Cl and loads. The measurement campaign should aim to obtain ~~a set of~~ measurements with a balanced distribution of ~~FA~~ these angles.

In section 7, the HAWC2 Near-Wake induction model (model accounting for the 3D effects due to the vorticity trailed from the edges and along the span of the flap section) does not ~~effect~~ affect the average transient of ΔCl and Δ~~MBrM as their~~ BMD as they differ respectively less than 4% and 1% compared to the HAWC2 model without Near-Wake. The Near-Wake model ~~impact marginally~~ impacts the value of Δ~~MBrM~~BMD marginally, reducing it between 2 to 2.5%. This reduction, even if small, ~~improve the accuracy of the model~~improves the model's accuracy to estimate the Δ~~MBrM~~ BMD as the HAWC2 model ~~overestimate~~ overestimates it, as shown in Gamberini et al. (2022). This result confirms the conclusions of Prospathopoulos et al. (2021), that a BEM model without 3D trailed vorticity effects overestimates the flap contribution at the flap location ~~as well as at~~ and the blade root~~, but the difference of~~ . However, the difference in the integral loads is rather small when the flap actuation frequency is below 1P, like in the validation described in the current paper.

Finally, the azimuth-based b2b method proved to be a reliable methodology to estimate the asymmetrical loading caused by the ATEF equipped on a single blade of the ~~PT~~Prototype. This methodology can be applied in other asymmetrical rotor loading conditions, for example, in case of individual pitch, pitch error, or blade degradation.

9 Conclusions

Within the framework of the VIAs project, an Active Trailing Edge Flap System was installed on a 4.3 MW test wind turbine and underwent a field test campaign for over 1.5 years. The campaign provided the measurement data to validate the aerodynamic ATEF ~~models~~ model of the aeroelastic engineering ~~tools BHawC and~~ tool BHawC and the more advanced ATEFlap model of HAWC2. The validation focused on the dynamic response of the ATEF models during flap actuation and consisted of three phases. At first, the flap actuator model was tuned to accurately reproduce the flap deflection ~~transient~~ during the 2 s activation and the 5 s deactivation. In the second phase, the aerodynamic flap model was tuned and validated through the lift coefficient ~~transients~~ transient responses measured at a blade section equipped with the flap. Finally, the aeroelastic ATEF model was validated under varying weather conditions based on the blade load ~~transients over a three month period~~transient responses over three months, from October to December ~~2020, with varying weather conditions.~~ 2020. A novel approach to computing the blade load impact of the flap was introduced. This method is an azimuth-based variation of the blade-to-blade approach, and it computes the difference between azimuthal synchronized loads of adjacent blades.

The validation showed that for the tested actuator model, the two aeroelastic ATEF models provide almost identical transients during flap activation and deactivation, with the main difference caused by a relative time shift lower than 0.04 s (~~one time step~~two time steps) between the Cl transients and below 0.08 s between the load transients. The validation showed that the ~~simulations transient~~ simulation transient responses of Cl and ~~MBrM~~ BMD are in good agreement with the corresponding measured ~~transients~~responses, confirming that the aeroelastic ATEF models provide a reliable and precise estimation of the impact of the flap on the wind turbine during flap actuation. In comparison with the field data, the maximum differences between the simulated and the measured Cl transient curves are below 8% of the ΔCl and within 0.15 s of time shift during flap activation, below 8% ΔCl and within 0.2 s of time shift during flap deactivation. Regarding the ~~MBrM transients~~BMD transient curves, the maximum difference is below 1% of the mean blade load during flap activation and below 1.7% during flap

deactivation, with a delay within $0.2\,\mathrm{s}$ for both flap actuation cases. Additional measurements of the flap deflection at different blade locations, under wide ~~WT operational conditions~~wind turbine operational conditions, and the direct measurement of the aerodynamic properties of all flap ~~profiles~~ airfoils are suggested solutions to ~~fine tune~~ fine-tune the ATEF model.

To the authors' knowledge, this validation is the most extensive published ~~validation~~ study of the aeroelastic ATEF model ~~transients~~ transient responses in terms of wind conditions, time, and flap size. This validation was enabled by measuring the aerodynamic response at a blade section during flap activation/deactivation with a unique inflow and pressure belt system. Combined with the complementary validation of the static properties of the aeroelastic ATEF model, this validation increases the safety and reliability of the aeroelastic design environment for the ~~WT~~ wind turbine equipped with active flaps~~and provides the basis~~. It provides a validated and reliable foundation for further exploration of the ATEF technology, a fundamental milestone in designing future wind turbines equipped with ATEF. Future research should aim to identify the limits of application of the ATEF models in terms, for example, of actuator performance (e.g., maximum speed or deflection) or external conditions (e.g., wind misalignment, extreme wind speed, or direction change).

Author contributions. A.Go conceived and planned the measurements with the support of A.Ga, T.Ba, and H.Ma. A.Go, and H.Ma performed the flyboard measurements. A.Go performed the extended validation measurements and the video recording of the flap deflection. A.Ga. performed the model tuning, the calculations, and the postprocessing, supported by T.Ba for the Cl extraction. A.Ga developed the az-b2b method from the initial b2b method developed by A.Go. A.Go and T.Ba supervised the project. All authors discussed the results. A.Ga. wrote the manuscript with input from all authors.

Competing interests. A.Ga. and A.Go. are hired by Siemens Gamesa Renewable Energy, company that is developing the flap technology used as reference in the paper.

Acknowledgements. This research was partially funded by Danmarks Innovationsfond, Case no. 9065-00243B, PhD Title: "Advanced model development and validation of Wind Turbine Active Flap system".

The Validation of Industrial Aerodynamic Active Add-ons (VIAs) project is a collaboration between Siemens Gamesa Renewable Energy, DTU Wind Energy and Rehau AS, partially funded by EUDP under journal nr. 64019-0061.

The authors thank ~~the anonymous reviewers~~ Pietro Bortolotti and an anonymous reviewer whose comments and suggestions helped improve and clarify this manuscript.

References

Aagaard Madsen, H., Andersen, P. B., Løgstrup Andersen, T., Bak, C., Buhl, T., and Li, N.: The potentials of the controllable rubber trailing edge flap (CRTEF), vol. 3, pp. 2165–2175, European Wind Energy Association (EWEA), 2010.

Aagaard Madsen, H., Juul Larsen, T., Raimund Pirrung, G., Li, A., and Zahle, F.: Implementation of the blade element momentum model on a polar grid and its aeroelastic load impact, Wind Energy Science, 5, 1–27, https://doi.org/10.5194/wes-5-1-2020, 2020.

Abbas, N. J., Bortolotti, P., Kelley, C., Paquette, J., Pao, L., and Johnson, N.: Aero-servo-elastic co-optimization of large wind turbine blades with distributed aerodynamic control devices, Wind Energy, https://doi.org/https://doi.org/10.1002/we.2840, 2023.

Andersen, P. B.: Advanced load alleviation for wind turbines using adaptive trailing edge flaps : sensoring and control, Risø National Laboratory, 2010.

Barlas, T., Pettas, V., Gertz, D., and Madsen, H. A.: Extreme load alleviation using industrial implementation of active trailing edge flaps in a full design load basis, in: Journal of Physics: Conference Series, vol. 753, Institute of Physics Publishing, https://doi.org/10.1088/1742-6596/753/4/042001, 2016.

Barlas, T. K., van Wingerden, W., Hulskamp, A., Van Kuik, G., and Bersee, H.: Smart dynamic rotor control using active flaps on a small-scale wind turbine: aeroelastic modeling and comparison with wind tunnel measurements, Wind Energy, 16, 1287–1301, https://doi.org/10.1002/we.1560, 2013.

Barlas, T. K., Olsen, A. S., Madsen, H. A., Andersen, T. L., Ai, Q., and Weaver, P. M.: Aerodynamic and load control performance testing of a morphing trailing edge flap system on an outdoor rotating test rig, Journal of Physics: Conference Series, 1037, 022 018, https://doi.org/10.1088/1742-6596/1037/2/022018, 2018.

Bartholomay, S., Krumbein, S., Deichmann, V., Gentsch, M., Perez-Becker, S., Soto-Valle, R., Holst, D., Nayeri, C. N., Paschereit, C. O., and Oberleithner, K.: Repetitive model predictive control for load alleviation on a research wind turbine using trailing edge flaps, Wind Energy, 25, 1290–1308, https://doi.org/10.1002/we.2730, 2022.

Bartholomay, S., Krumbein, S., Perez-Becker, S., Soto-Valle, R., Nayeri, C. N., Paschereit, C. O., and Oberleithner, K.: Experimental assessment of a blended fatigue-extreme controller employing trailing edge flaps, Wind Energy, 26, 201–227, https://doi.org/10.1002/we.2795, 2023.

Berg, J. C., Barone, M. F., and Resor, B. R.: Field test results from the Sandia SMART rotor, 51st Aiaa Aerospace Sciences Meeting Including the New Horizons Forum and Aerospace Exposition 2013, 2013.

Bergami, L. and Gaunaa, M.: ATEFlap Aerodynamic Model, a dynamic stall model including the effects of trailing edge flap deflection, Danmarks Tekniske Universitet, Risø Nationallaboratoriet for Bæredygtig Energi, 2012.

Bergami, L. and Poulsen, N. K.: A smart rotor configuration with linear quadratic control of adaptive trailing edge flaps for active load alleviation, Wind Energy, 18, 625–641, https://doi.org/10.1002/we.1716, 2015.

Bernhammer, L. O., van Kuik, G. A., and De Breuker, R.: Fatigue and extreme load reduction of wind turbine components using smart rotors, Journal of Wind Engineering and Industrial Aerodynamics, 154, 84–95, https://doi.org/https://doi.org/10.1016/j.jweia.2016.04.001, 2016.

Bossanyi, E.: GH Bladed–Theory Manual, Version 4.4, Garrad Hassan and Partners, 2013.

Brown, D., Christian, W., and Hanson, R. M.: Tracker, video analyses and modelling tool, https://physlets.org/tracker/, 2023.

Castaignet, D., Buhl, T., Poulsen, N. K., and Wedel-Heinen, J. J.: Trailing edge flaps impact on fatigue and extreme loads in power production, EWEA 2011, 2011.

Castaignet, D., Barlas, T. K., Buhl, T., Poulsen, N. K., Wedel-Heinen, Jens, J., Olesen, N. A., Bak, C., and Kim, T.: Full-scale test of trailing edge flaps on a Vestas V27 wind turbine: active load reduction and system identification, Wind Energy, 17, 549–564, https://doi.org/10.1002/we.1589, 2014.

Ferreira, C., Gonzalez, A., Baldacchino, D., Aparicio, M., Gómez, S., Munduate, X., Garcia, N. R., Sørensen, J. N., Jost, E., Knecht, S., Lutz, T., Chassapogiannis, P., Diakakis, K., Papadakis, G., Voutsinas, S., Prospathopoulos, J., Gillebaart, T., and Van Zuijlen, A.: Results of the AVATAR project for the validation of 2D aerodynamic models with experimental data of the DU95W180 airfoil with unsteady flap, in: Journal of Physics: Conference Series, vol. 753, Institute of Physics Publishing, https://doi.org/10.1088/1742-6596/753/2/022006, 2016.

Fischer, A. and Aagaard Madsen, H.: Investigation of the theoretical load alleviation potential using trailing edge flaps controlled by inflow data, Wind Energy, 19, 1567–1583, https://doi.org/10.1002/we.1937, 2016.

Fisker Skjoldan, P.: Aeroelastic modal dynamics of wind turbines including anisotropic effects, Risø National Laboratory, 2011.

Gamberini, A., Gomez Gonzalez, A., and Barlas, T.: Aeroelastic model validation of an Active Trailing Edge Flap System tested on a 4.3 MW wind turbine, Journal of Physics. Conference Series, 2265, 032 014, https://doi.org/10.1088/1742-6596/2265/3/032014, 2022.

Gomez Gonzalez, A., Enevoldsen, P. B., Akay, B., Barlas, T. K., Fischer, A., and Aa Madsen, H.: Experimental and numerical validation of active flaps for wind turbine blades, in: Journal of Physics: Conference Series, vol. 1037, Institute of Physics Publishing, https://doi.org/10.1088/1742-6596/1037/2/022039, 2018.

Gomez Gonzalez, A., Bay Enevoldsen, P., Barlas, A., and Madsen, H. A.: General rights Field test of an active flap system on a full-scale wind turbine Field test of an active flap system on a full-scale wind turbine, Wind Energ. Sci, 6, 33–43, https://doi.org/10.5194/wes-6-33-2021, 2021.

Gomez Gonzalez, A., Enevoldsen, P., Barlas, T., and Madsen, H. A.: Test of an active flap system on a 4.3 MW wind turbine, Journal of Physics. Conference Series, 2265, 032 016, https://doi.org/10.1088/1742-6596/2265/3/032016, 2022.

Gonzalez, A. G., Enevoldsen, P., Barlas, T. K., Madsen, H. A., and Olsen, A. S.: Consolidated results of the laboratory and full scale field validation of an active flap system, Journal of Physics: Conference Series, 1618, 52 024, https://doi.org/10.1088/1742-6596/1618/5/052024, 2020.

Jonkman, J. M., Buhl, M. L., et al.: FAST user's guide, vol. 365, National Renewable Energy Laboratory Golden, CO, USA, 2005.

Lackner, M. A. and Van Kuik, G.: A comparison of smart rotor control approaches using trailing edge flaps and individual pitch control, Wind Energy, 13, 117–134, https://doi.org/10.1002/we.353, 2010.

Larsen, T. J. and Hansen, A. M.: How 2 HAWC2, the user's manual, 2023.

Madsen, H. A., Barlas, T., Fischer, A., Olsen, A. S., and Gomez Gonzalez, A.: Inflow and pressure measurements on a full scale turbine with a pressure belt and a five hole pitot tube, Journal of Physics: Conference Series, 2265, https://doi.org/10.1088/1742-6596/2265/2/022096, 2022.

Pettas, V., Barlas, T., Gertz, D., and Madsen, H. A.: Power performance optimization and loads alleviation with active flaps using individual flap control, in: Journal of Physics: Conference Series, vol. 749, p. 012010, Institute of Physics Publishing, https://doi.org/10.1088/1742-6596/749/1/012010, 2016.

Pirrung, G., Riziotis, V., Madsen, H., Hansen, M., and Kim, T.: Comparison of a coupled near- And far-wake model with a free-wake vortex code, Wind Energy Science, 2, 15–33, https://doi.org/10.5194/wes-2-15-2017, 2017.

Prospathopoulos, J. M. et al.: Simulation of oscillating trailing edge flaps on wind turbine blades using ranging fidelity tools, Wind Energy, 24, 357–378, https://doi.org/10.1002/we.2578, 2021.

Ungurán, R. and Kühn, M.: Combined individual pitch and trailing edge flap control for structural load alleviation of wind turbines, Proceedings of the American Control Conference, 2016-, 2307–2313, https://doi.org/10.1109/ACC.2016.7525262, 2016.

Van Wingerden, J. W., Hulskamp, A. W., Barlas, T., Marrant, B., Van Kuik, G. A., Molenaar, D. P., and Verhaegen, M.: On the proof of concept of a 'smart' wind turbine rotor blade for load alleviation, Wind Energy, 11, 265–280, https://doi.org/10.1002/we.264, 2008.